Anatomical and Ultrastructural Characterization of the Frog Accessory Olfactory Bulb and Vomeronasal Nerve

by

Xander Merx

A Thesis Submitted in Partial Fulfillment of the
Requirements for the Degree of

BACHELOR OF SCIENCE (HONS.)

in the Department of Biology

University of Victoria

Anatomical and Ultrastructural Characterization of the Frog Accessory Olfactory Bulb and Vomeronasal Nerve

by

Xander Merx

<u>Supervisory Committee</u>

Dr. Kerry Delaney, Supervisor
Department of Biology

Dr. Raad Nashmi, External Examiner
Department of Biology

Dr. Barbara Hawkins, Honours Advisor
Department of Biology

Abstract

The accessory olfactory bulb (AOB) serves as the central relay for vomeronasal chemosensory information and has been implicated in activity-dependent synaptic plasticity in frogs. Activity-dependent enhancement (ADE), observed at the vomeronasal nerve (VNN)–mitral cell synapse, has been described in *Rana pipiens* and hypothesized to involve neuropeptide co-release from dense-core vesicle (DCV)-containing afferent terminals. Bimodal compound action potential recordings from the *Lithobates catesbeiana* VNN suggest the presence of two morphologically distinct axon populations. The present study employed light microscopy, transmission electron microscopy (TEM), and horseradish peroxidase (HRP) anterograde tracing to characterize the anatomy and ultrastructure of the AOB and VNN in adult *L. catesbeiana*.

Light microscopy revealed a laminated AOB with glomerular and mitral cell layers; a notably sparse periglomerular cell population was identified, consistent with the frog AOB being less elaborated than its mammalian counterpart. TEM of the glomerular neuropil identified likely dendrodendritic synapses and gap junctions, features documented in the mammalian olfactory bulb but not previously reported in the frog AOB. Large vesicular profiles with electron-dense cores were observed in HRP-DAB labeled VNN afferent terminals; however, the evidence is insufficient to confirm the presence of dense-core vesicles, and these observations do not provide anatomical support for the neuropeptide co-release hypothesis. Quantitative axon diameter analysis identified two morphologically distinct fascicle types: Type A fascicles with a unimodal small-axon distribution and Type B fascicles with a bimodal distribution with a sparse large-profile subpopulation, consistent with the bimodal CAP profile.

These structural observations support ongoing functional investigations and warrant further study using biochemical and volumetric imaging approaches.

Table of Contents

List of Figures

Acknowledgements

I would like to thank my supervisor, Dr. Kerry Delaney, for his guidance, support, and intellectual contributions throughout this project, and for performing dissections, vibratome sectioning, HRP nerve filling, and DAB reactions used in this study.

I am deeply grateful to Sammy Weiser Novak, manager of the University of Victoria Biology Electron Microscopy Facility, for training and extensive technical assistance, for performing osmium staining, dehydration, resin infiltration and embedding, semithin section staining, light microscopic imaging, and transmission electron microscopy, and for invaluable guidance on thesis preparation and scientific writing. The Biology EM Facility provided essential infrastructure and expertise without which this work would not have been possible.

I would like to thank Dr. Bob Chow for generously providing access to the Nikon Eclipse TE2000-U light microscope used for semithin section imaging.

I would also like to thank Dr. Raad Nashmi for serving as the external examiner of my thesis.

Introduction

1.1 The Olfactory System

The vertebrate chemosensory system is organized into two anatomically and functionally distinct major subsystems: the main olfactory system and the accessory olfactory system. The two systems differ not only in receptor neuron morphology and central connectivity but also in the nature of the stimuli they transduce and in the behavioural and neuroendocrine responses they mediate. The main olfactory system detects volatile chemical stimuli via ciliated sensory neurons in the main olfactory epithelium (MOE), which project to the main olfactory bulb (MOB) and from there to the olfactory cortex, olfactory amygdala, and associated areas (Mucignat-Caretta, 2010). The accessory olfactory system, by contrast, detects a broader range of chemosignals, including many non-volatile and some volatile molecules, peptides, and species-specific compounds, through microvillar sensory neurons of the vomeronasal organ (VNO), whose axons project to the accessory olfactory bulb (AOB) and from there primarily to the vomeronasal amygdala and hypothalamus (Mucignat-Caretta, 2010; Fig. 1).

The presence of a discrete vomeronasal system, anatomically separate from the main olfactory system, is a derived character in tetrapods (Eisthen, 1992). Phylogenetic analysis using cladistic methods indicates that the system most likely originated with early amphibians, as separate olfactory and vomeronasal systems are demonstrable in aquatic larval amphibians across all three amphibian orders (anurans, urodeles, and caecilians) as well as in metamorphosed aquatic adults (Eisthen, 1992). The presence of the vomeronasal system prior to metamorphosis in these groups argues against the hypothesis that the system arose as an adaptation to terrestrial life (Eisthen, 1992). The system has been secondarily lost in several tetrapod lineages, including crocodilians, birds, cetaceans, and some primates, while being retained in the majority of terrestrial and semi-aquatic tetrapods (Eisthen, 1992; Mucignat-Caretta, 2010).

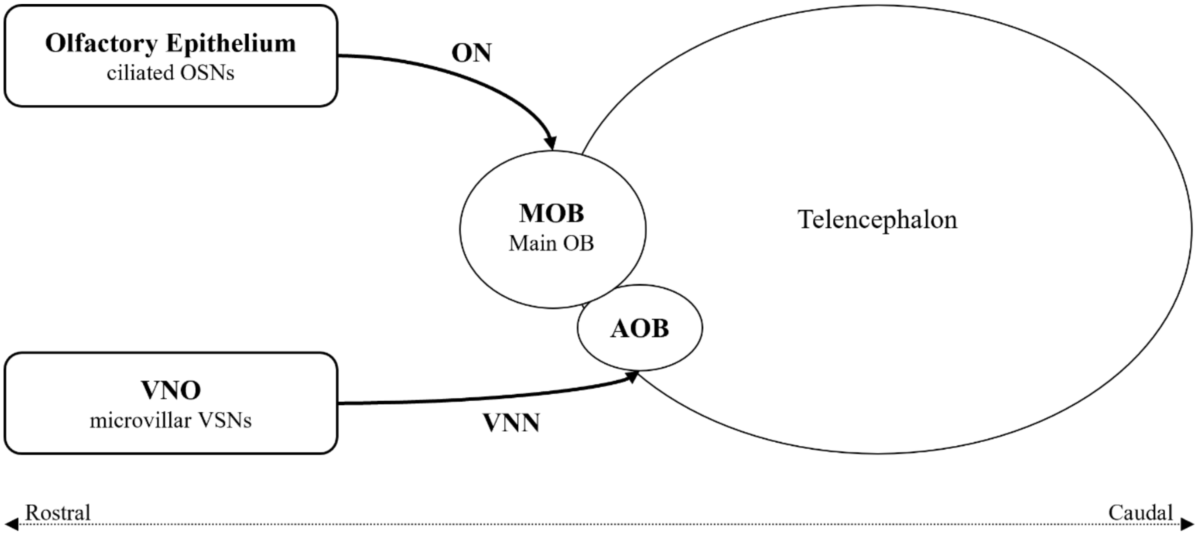

Figure 1. Schematic overview of the main and accessory olfactory pathways in *Lithobates catesbeiana*. The main olfactory system detects volatile chemosignals via ciliated olfactory sensory neurons (OSNs) in the olfactory epithelium, whose axons project along the olfactory nerve (ON) to the main olfactory bulb (MOB). The accessory olfactory system detects a broader range of chemosignals via microvillar vomeronasal sensory neurons (VSNs) in the vomeronasal organ (VNO), whose axons project along the vomeronasal nerve (VNN) to the accessory olfactory bulb (AOB), located on the ventral surface of the MOB. Both bulbs are situated at the rostral pole of the telencephalon.

Despite broad conservation of the basic vomeronasal circuit architecture across tetrapods, the accessory olfactory system has been most thoroughly characterized in rodents, where its roles in pheromone detection, mate recognition, and reproductive physiology have been extensively studied (Mucignat-Caretta, 2010). Comparative data from non-mammalian tetrapods, including anuran amphibians, remain limited. *Lithobates (Rana) catesbeiana* (American bullfrog) offers a particularly valuable model for examining the accessory olfactory system in a non-mammalian tetrapod, given the tractability of its anatomy and the availability of electrophysiological data from the Delaney laboratory establishing neural circuit properties of the AOB and amygdala in closely related ranid frogs (Mulligan et al., 2001; Delaney et al., 2009). The present study extends the ultrastructural characterization of the AOB in *L. catesbeiana* initiated by Burton (1990), employing horseradish peroxidase-loading of the VNN to confirm terminal origin, semithin histology, and quantitative analysis of the VSN axons to address outstanding questions about circuit organization and synaptic composition.

1.2 The Vomeronasal Organ and Vomeronasal Nerve

The vomeronasal organ (VNO) is a paired chemosensory structure present in most tetrapods. It is lined by a sensory epithelium populated by bipolar vomeronasal sensory neurons (VSNs), whose microvillar dendrites extend toward the lumen of the organ and whose axons fasciculate to form the vomeronasal nerve (VNN) (Eisthen, 1992). In mammals, VSNs are organized into apical and basal subpopulations expressing distinct receptor gene families (V1Rs and V2Rs, respectively) and projecting to anterior and posterior subdivisions of the AOB (Mucignat-Caretta, 2010; Ishii et al., 2003). In anuran amphibians, the VNO is present throughout the lifecycle, including in aquatic larval stages, indicating that it is not a terrestrial adaptation and that its function is not restricted to airborne chemosignal detection (Eisthen, 1992). The receptor neuron populations and molecular organization of the anuran VNO are less thoroughly characterized than those found in mammals and the receptor gene families expressed by VSNs remain to be described. The sensory epithelium of the anuran VNO contains microvillar receptor cells, consistent with the ancestral condition identified across tetrapods (Eisthen, 1992).

The axons of VSNs project ipsilaterally via the VNN to the glomerular layer of the AOB, where they form axodendritic synapses onto the apical dendrites of mitral cells (Burton, 1990; Burton et al., 1990). This projection constitutes the primary afferent input to the AOB and represents the first synaptic relay in the accessory olfactory pathway. In *L. catesbeiana*, the morphology and termination pattern of the VNN have been described in detail by Burton and colleagues (Burton, 1990; Burton et al., 1990), who characterized the axonal projection using light microscopy and electron microscopy in both larval and adult animals. These studies established that VSN axons terminate in discrete glomeruli within the AOB and provided the most detailed anatomical data available for any ranid frog. The present study extends this comparative framework by characterizing the fine structure of VNN terminals and their postsynaptic partners at the ultrastructural level in *L. catesbeiana* using TEM and by employing HRP-DAB anterograde tracing to confirm which synaptic structures seen in TEM are from VNN afferents.

Whether axon diameter uniformity exists in the anuran VNN has not been established. Compound action potential recordings from the VNN of *L. catesbeiana* conducted in the Delaney laboratory have revealed two distinct peaks in the conduction velocity profile, consistent with the presence of two populations of axons with differing conduction velocities (K. Delaney, unpublished data). Axon conduction velocity generally scales with axon diameter, such that bimodal conduction velocity distributions predict bimodal axon diameter distributions (Augustine et al., 2023). If two morphologically distinct axon populations are present in the VNN of *L. catesbeiana*, this would suggest either the existence of VSN subtypes with distinct physiological properties, or the presence of a non-sensory axon population within the nerve. The present study uses quantitative TEM-based axon diameter measurements to determine whether the ultrastructural composition of the VNN is consistent with two distinct axon populations, providing a morphological basis for interpreting the electrophysiological observations.

1.3 The Accessory Olfactory Bulb

The accessory olfactory bulb (AOB) is a laminated structure situated on the posterodorsal surface of the main olfactory bulb in most tetrapods. It receives the primary afferent projection from the VNO via the VNN and serves as the first central relay in the accessory olfactory pathway. The AOB is conventionally divided into several layers (from lateral to medial): the nerve fibre layer, containing unmyelinated VNN axons; the glomerular layer, where axodendritic synapses are formed between VSN terminals and the apical dendrites of mitral and tufted cells; the mitral cell layer; and the granule cell layer, which contains GABAergic interneurons (Halpern & Martínez-Marcos, 2003). Unlike the MOB, AOB glomeruli exhibit greater convergence of sensory inputs, receiving input from VSN axons of more than one receptor type and being contacted by the apical dendrites of multiple mitral cells, a feature thought to enable combinatorial processing of complex chemosensory stimuli (Mucignat-Caretta, 2010). The primary output neurons of the AOB, the mitral cells, project via the accessory olfactory tract to the vomeronasal amygdala and from there to the hypothalamus and other limbic structures, providing the substrate for the neuroendocrine and reproductive responses mediated by the accessory olfactory system (Mucignat-Caretta, 2010).

At the ultrastructural level, the synaptic organization of the AOB has been characterized primarily in rodents using TEM. These studies describe that a glomerular layer contains asymmetric axodendritic synapses formed by VSN terminals onto mitral cell apical dendrites; these terminals contain small clear vesicles consistent with fast neurotransmitter release (Jia et al., 1999; Quaglino et al., 1999). DCVs alongside the more abundant lucent vesicles have been documented in VNN axon terminals in the glomerular layer of the bullfrog AOB and are consistent with co-release of neuropeptides alongside classical neurotransmitters, a feature with potential implications for synaptic plasticity (Burton, 1990); DCVs have also been identified in GABAergic periglomerular profiles in the mammalian MOB glomerular layer (Toida et al., 1998). The granule cell layer contains reciprocal dendrodendritic synapses between granule cell spines and mitral cell lateral dendrites, providing both recurrent inhibition and lateral inhibition between mitral cells (Bartel et al., 2015). Likely gap junctions between mitral cell dendrites have been documented ultrastructurally in the olfactory bulb, where they are proposed to contribute to synchronization of mitral cell activity within glomeruli (Christie et al., 2005; Bourne & Schoppa, 2017; Maher et al., 2009). These ultrastructural features collectively define the synaptic substrate through which the AOB processes and transforms vomeronasal input. While dendrodendritic synapses have been documented in the frog AOB (Burton, 1990), gap junctions have not been reported in the anuran AOB and the relationship between these features and how they appear in mammals remains incompletely characterized. Further ultrastructural investigation in *L. catesbeiana* is therefore warranted (Fig. 2).

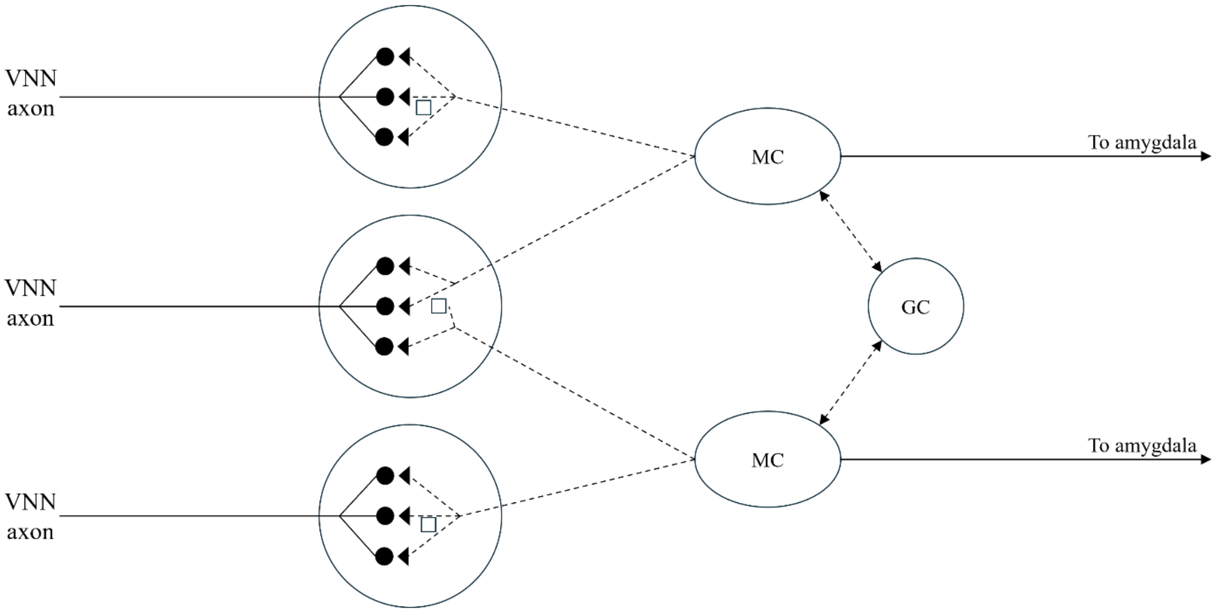

Figure 2. Schematic of vomeronasal circuit organization in *Lithobates catesbeiana*. Three vomeronasal nerve (VNN) axons project to separate glomeruli, forming axodendritic synapses (filled circles with arrowheads) onto the apical dendrites (dashed lines) of mitral cells (MC). Each mitral cell extends apical dendrites to multiple glomeruli. Mitral cell dendrites form dendrodendritic contacts (open squares) with one another, and reciprocal dendrodendritic connections (bidirectional arrows) with granule cells (GC), providing recurrent inhibition. Mitral cell axons project via the accessory olfactory tract to the amygdala.

1.4 The Accessory Olfactory Bulb in Anuran Amphibians

Anuran amphibians occupy a phylogenetically prominent position for understanding the evolution of the accessory olfactory system. As non-amniote tetrapods, anurans provide a comparative outgroup against which the derived features of the mammalian AOB can be evaluated (Eisthen, 1992). The AOB has been documented in anurans across multiple species and its laminar organization and afferent connectivity have been described at the light and electron microscopic levels in several species of ranid frogs (Kemali & Guglielmotti, 1987; Scalia et al., 1991; Burton, 1990; Burton et al., 1990).

The anuran AOB has been observed at the light microscopic level to possess a glomerular zone receiving VNN input and an associated population of output neurons whose axons project caudally via the accessory olfactory tract, features broadly consistent with the mammalian AOB organization (Kemali & Guglielmotti, 1987). However, the degree of laminar differentiation and the complement of cell types present in the anuran AOB may differ from that of rodents and comparative ultrastructural data are scarce. The present study extends the anatomical characterization of the *L. catesbeiana* AOB through semithin section histology by light microscopy, ultrathin section histology by transmission electron microscopy (TEM), and HRP-loading of VNN axons for identifying VNN afferents in the glomerular neuropil by TEM.

L. catesbeiana is a well-established model organism in physiological and neuroanatomical research, and its brain anatomy including the AOB and VNN is well-suited to dissection, vibratome sectioning, and both light and electron microscopic analysis. Electrophysiological properties of the AOB, including activity-dependent enhancement, have been investigated in the closely related ranid *Rana pipiens* in the Delaney laboratory (Delaney et al., 2009; Mulligan et al., 2001). While Burton (1990) provided an initial ultrastructural characterization of the AOB in *L. catesbeiana*, including synaptic profiles and vesicle populations, a systematic description of laminar organization using semithin histology, HRP-confirmed terminal identity at the ultrastructural level, and quantitative analysis of VNN axon composition has not been reported. The present study addresses these gaps, providing a baseline anatomical description of the AOB in *L. catesbeiana* that supports ongoing electrophysiological investigation of activity-dependent plasticity in this circuit.

1.5 Activity-Dependent Enhancement in the Accessory Olfactory Bulb

Activity-dependent enhancement (ADE) is a form of use-dependent plasticity in the AOB of *R. pipiens* characterized by a progressive increase in the amplitude of field potential responses evoked by repeated or sustained stimulation of the VNN (Delaney et al., 2009). Unlike classical long-term potentiation, which typically requires high-frequency tetanic stimulation, ADE in the *R. pipiens* AOB can be induced by stimulus protocols that more closely resemble naturalistic patterns of vomeronasal nerve activity (Delaney et al., 2009). This property suggests that ADE may be physiologically relevant during sustained or repeated chemosensory exposure, with potential implications for processes such as mate recognition, habituation, or sensitization to conspecific chemosignals. ADE has been documented electrophysiologically in the Delaney laboratory and represents the primary functional context motivating the present anatomical study (Delaney et al., 2009).

The cellular and subcellular mechanisms underlying ADE remain to be fully characterized. Several candidate mechanisms can be proposed on the basis of what is known about synaptic organization in the AOB more broadly. Modulation of dendrodendritic synaptic efficacy in the granule cell layer could alter the balance of recurrent inhibition onto mitral cells, thereby enhancing net output. Alternatively, activity-dependent release of neuropeptides from DCVs in presynaptic terminals could produce sustained neuromodulatory effects on circuit excitability through metabotropic signaling pathways. Electrical coupling between mitral cells via gap junctions could also contribute to synchronization and amplification of population responses (Maher et al., 2009). Each of these mechanisms has a distinct ultrastructural correlate that can be identified and characterized by TEM. The present study does not seek to establish a causal link between any specific ultrastructural feature and ADE but rather provides the anatomical foundation necessary to evaluate these candidate mechanisms and to interpret ongoing electrophysiological experiments within a structural framework.

1.6 Rationale and Objectives

The synaptic basis of ADE at the VNN–mitral cell synapse in ranid frogs remains unresolved. Delaney et al. (2009) reported that ADE is consistent with a presynaptic mechanism and persists following reduction of extracellular calcium, findings that may argue against classical residual-calcium–dependent enhancement mechanisms. A candidate mechanism consistent with these properties is activity-dependent co-release of neuropeptides from dense-core vesicles (DCVs) in VNN afferent terminals, which could produce sustained neuromodulatory effects on circuit excitability through metabotropic signaling pathways. However, whether DCVs are present in VNN afferent terminals in *Lithobates catesbeiana* has not been established and anatomical confirmation of their presence is a prerequisite to mechanistic interpretation. More broadly, while Burton (1990) provided an initial ultrastructural characterization of the *L. catesbeiana* AOB, a systematic description integrating semithin histology, HRP-DAB confirmed terminal identity, and quantitative VNN axon analysis has not been reported, limiting structural interpretation of physiological findings and precluding meaningful comparison with the better-characterized AOBs of other vertebrate taxa.

The objective of this thesis was to provide an anatomical and ultrastructural characterization of the AOB and vomeronasal nerve in *L. catesbeiana* using light microscopy (LM) and transmission electron microscopy (TEM). Specific objectives were: (1) to describe the gross anatomical organization and laminar structure of the AOB using semithin LM sections; (2) to characterize the ultrastructure of the AOB glomerular layer, including synaptic profiles, vesicle populations, dense-core vesicles, dendrodendritic contacts, and likely gap junctions; (3) to confirm the axonal projection of the vomeronasal nerve to the AOB glomerular layer using HRP-DAB tract tracing; (4) to contextualize these findings comparatively within the broader vertebrate AOB literature, with particular reference to the anatomical substrate of ADE; and (5) to determine whether the vomeronasal nerve of *L. catesbeiana* contains two morphologically distinct axon populations based on axon diameter, as predicted by unpublished electrophysiological recordings from the Delaney laboratory showing two peaks in the compound action potential profile of the VNN (K. Delaney, unpublished data).

We hypothesize that VNN afferent terminals in the AOB of *L. catesbeiana* contain dense-core vesicles, consistent with the capacity for neuropeptide co-release as a presynaptic mechanism underlying activity-dependent enhancement. We further hypothesize that the VNN contains two morphologically distinct axon populations distinguishable by cross-sectional diameter, consistent with the bimodal compound action potential profile recorded from this nerve.

Materials and Methods

2.1 Statement of Work

The following procedures were undertaken personally by the author as part of the practical training component of this Honours thesis. I performed dissections of adult *Lithobates catesbeiana* to remove the brain and associated olfactory nerves. I performed agarose embedding of fixed tissue, vibratome sectioning, and collection of sections for further processing. I manufactured glass knives for sectioning epoxy-embedded tissues. I trimmed blocks and cut semithin sections with a glass knife using an ultramicrotome. I performed several HRP vomeronasal nerve-filling procedures. I supported sample preparation and imaging for light microscopy. I determined regions of interest and acquired images using the JEOL JEM-1011 transmission electron microscope (JEOL Ltd., Tokyo, Japan), and the Gatan Rio 9 camera and Digital Micrograph software (Gatan Inc., Pleasanton, U.S.A). I performed image analysis in FIJI/ImageJ (Schindelin et al., 2012). I assembled figures in PowerPoint (Microsoft Corporation, Redmond, USA) and Photoshop (Adobe Inc., Adobe Systems, San Jose, USA). Additional procedures including dissection, vibratome sectioning, HRP filling and DAB reactions, osmium staining, dehydration, resin infiltration and embedding, semithin section staining, light microscopic imaging, ultrathin sectioning, and TEM imaging were performed by Dr. K. Delaney and S. Weiser Novak (Biology EM Facility).

2.2 Animals

Adult American bullfrogs (*Lithobates catesbeiana*) of both sexes were used for all experiments. Animals were maintained in the animal care facility at the University of Victoria. All procedures were conducted in accordance with the guidelines of the Canadian Council on Animal Care and approved by the University of Victoria Animal Care Committee (Protocol No. AE-2023-011).

2.3 Tissue Preparation and Fixation

Adult frogs were deeply anaesthetized by immersion in tricaine methanesulfonate (MS-222; 0.3%, buffered to pH 7.0 with sodium bicarbonate) until loss of righting reflex and cessation of response to physical stimuli. Two tissue preparation procedures were undertaken depending on the experimental aim.

For histological and ultrastructural analyses (i.e., without HRP-DAB reactions), the brain including the olfactory and vomeronasal nerves was rapidly dissected and transferred into fixative solution composed of 2.5% glutaraldehyde, 2% paraformaldehyde, 2 mM $CaCl_2$, and 3% mannitol in 0.15 M sodium cacodylate buffer (pH 7.4, ~445 mOsm), maintained at 4°C prior to use (as described in Karlupia et al., 2023). After overnight fixation at 4°C, tissue was rinsed three times in PBS and stored at 4°C for two days prior to vibratome sectioning.

For HRP tract tracing experiments, the intact brain was removed as described above and transferred into frog Ringer's solution within approximately five minutes of euthanasia. A solution of HRP was applied to the cut stump of the vomeronasal nerve as described below (see Horseradish Peroxidase Tract Tracing). Following the HRP-loading period, tissue was fixed overnight at 4–6°C in the fixative solution described above, then rinsed and stored in PBS prior to vibratome sectioning.

2.4 Vibratome Sectioning

Fixed brains were embedded in 3% agarose prepared in PBS and allowed to solidify at room temperature. Coronal sections were cut using a vibratome in a bath of ice-cold PBS. The agarose embedded brain was secured to the plate of the vibratome using Krazy Glue, oriented so that the olfactory nerve would be cut first. Initial preparations were sectioned at 75 µm. Subsequent preparations were sectioned at 100 µm to improve tissue integrity during further tissue processing steps. Sections were collected into wells filled with PBS and examined under a stereomicroscope to identify the presence of the accessory olfactory bulb and vomeronasal nerve prior to further processing. Sections of interest were then sunk overnight in cryoprotectant solution composed of 4 parts PBS, 3 parts glycerol, and 3 parts ethylene glycol, and stored at -20°C until further osmium processing.

2.5 Osmium Staining, Dehydration, and Resin Embedding

Vibratome sections containing the VNN or AOB were thoroughly rinsed in PBS before further processing. To enhance membrane contrast and tissue fixation, samples were treated with a buffered reduced osmium solution composed of 4% osmium tetroxide (OsO_4), 10% potassium ferrocyanide ($K_4[Fe(CN)_6]$), and 0.15 M cacodylate buffer for 1 hour at room temperature. Following osmium treatment, sections were rinsed six times in distilled water. Sections were dehydrated through a graded ethanol series: 30% ethanol for 10 minutes, followed by 50% ethanol containing 2% aqueous uranyl acetate (1:1 v/v) for 1 hour to provide further *en bloc* heavy metal staining, then 70%, 90%, and 100% × 2 ethanol for 10 minutes each on ice, followed by two additional changes of 100% ethanol at room temperature.

Dehydrated sections were infiltrated with Epon 812 (hard formulation) epoxy resin through a graded series: 1:3 resin:ethanol overnight, 3:1 resin:ethanol for 4 hours, 100% resin for 2 hours, 100% resin overnight, and a final change of 100% resin for 2 hours. Sections were flat-embedded in BEEM capsules and polymerized at 60°C for 48 hours.

2.6 Light Microscopy

Semithin sections (500 nm) were cut from resin-embedded blocks using a Leica ultramicrotome (Leica Microsystems, Wetzlar, Germany) equipped with a glass knife or Diatome Histo Jumbo diamond knife (Diatome, Biel, Switzerland) and mounted onto glass slides. Mounted sections were dried on a hot plate prior to staining.

Sections were stained using a modified azure B–basic fuchsin protocol (Morikawa et al., 2018). Briefly, a working stain was prepared by mixing solution A (0.035% azure B and 0.015% basic fuchsin in 5% aqueous ethanol, prepared from 0.05% stock solutions at a 7:3 v/v ratio) with solution B (0.1 M sodium tetraborate) at a ratio of 5:1 (A:B v/v) no more than 20 min before use. Glass slides were preheated to 100°C on a hot plate, the working stain was applied to cover sections and slides were incubated for 30 s at 100°C. Stain was removed by rinsing with distilled water.

Stained sections were imaged in brightfield mode using a Nikon Eclipse TE2000-U (Nikon Ltd., Tokyo, Japan) microscope with a Plan Apo 20× (0.75NA) objective with additional 1.5x magnification with a final pixel size of 80 nm. These images were used to characterize tissue organization, laminar boundaries, and glomerular distribution across the AOB and to guide selection of regions of interest for further TEM imaging. Images were acquired using NIS Elements software (Nikon Ltd., Tokyo, Japan).

2.7 Transmission Electron Microscopy

Ultrathin sections were cut to a target thickness of 60–100 nm, as indicated by silver interference colour, from the same resin-embedded tissue blocks using an RMC Powertome ultramicrotome

(RMC Products, Tucson, USA) equipped with a Diatome Histo Jumbo diamond knife and collected onto Formvar-coated slot grids or 200-mesh copper grids. Heavy metal contrast was provided by the *en bloc* osmium and uranyl acetate processing steps described above; no additional post-staining was used. Grids were examined using a JEOL JEM-1011 transmission electron microscope operating at 80 kV. Images were acquired at magnifications ranging from 1,000–80,000× using a Gatan Rio 9 camera to document glomerular ultrastructure, synaptic vesicle populations, dense-core vesicles, synaptic profiles, and likely gap junctions within the AOB.

2.8 Horseradish Peroxidase Tract Tracing

To label the vomeronasal nerve projection to the AOB, horseradish peroxidase (HRP) was applied to the cut stump of the vomeronasal nerve to allow anterograde axonal transport to the AOB. A solution of approximately 30% HRP (w/v) in 2% dimethylsulfoxide (DMSO) was drawn up into a plastic tube fitted to the diameter of the vomeronasal nerve stump. The preparation was then perfused with frog Ringer's solution continuously bubbled with 95% O_2/5% CO_2 for 6 hours at room temperature to maintain oxygenation and pH during filling, then immersed overnight in 95% O_2/5% CO_2-saturated Ringer's solution in a sealed container at 4–6°C. Following the filling period, tissue was fixed overnight at 4–6°C in the fixative solution described above, then rinsed and stored in phosphate-buffered saline (PBS) with several solution changes and an overnight soak at 4–6°C. Vibratome sectioning of the brain prior to DAB-reaction with HRP facilitated developing reaction product in deeper brain regions.

HRP reaction product was visualized using a cobalt- and nickel-intensified 3,3'-diaminobenzidine (DAB) protocol. Tissue sections were soaked in a solution of 1% cobalt chloride and 1% nickel chloride for 15 minutes, after which the solution was discarded. Sections were then incubated in 3 mg/ml DAB in PBS (pH 7.4) for 10 minutes, followed by addition of 0.5–1% hydrogen peroxide (H_2O_2) for up to 10 minutes until a dark reaction product was visible. The DAB solution was then discarded into a waste container and neutralized with 10% sodium hypochlorite (bleach) solution. Sections of interest were stored at -20°C in cryoprotectant solution as described above. This method was employed to confirm the axonal projection pattern of vomeronasal sensory neurons to the glomerular layer of the AOB.

2.9 Image Analysis

All image analysis was performed using FIJI. Photoshop was used for figure preparation including image montaging and annotation. PowerPoint was used to assemble figure plates and further annotation. Quantitative TEM-based measurements were performed on cross-sectional profiles of VSN axons to determine the frequency distribution of the population and to evaluate whether the ultrastructural evidence supported the bimodal distribution predicted by previous electrophysiological recordings (K. Delaney, unpublished data). Axons with circular profiles were selected and their minimum diameters were measured manually from TEM images using FIJI. Individual axon profiles were identified by their visible boundaries and measured using the straight-line tool. A total of 609 axon profiles were measured from one Type A fascicle and 519 from one Type B fascicle, each from a single nerve preparation.

Results

3.1 Gross Morphology and HRP Localization of the Vomeronasal Pathway

The American bullfrog, *Lithobates catesbeiana*, was used as the experimental animal throughout this study; both sexes were used (Fig. 3A). To establish the trajectory and termination zone of the vomeronasal nerve (VNN) within the olfactory bulb, horseradish peroxidase (HRP) was applied to the cut stump of the vomeronasal nerve and allowed to undergo anterograde transport following dissection and prior to DAB reaction. In lateral views of the isolated brain, DAB reaction product was tightly localized to the accessory olfactory bulb (AOB) and VNN, with no labeling observed in the remainder of the telencephalon (Fig. 3B). At higher magnification, the reaction product resolved into two components: a discrete deposit on the ventral aspect of the olfactory bulb, corresponding to the AOB, and a dark fiber tract corresponding to the VNN, projecting into the AOB (Fig. 3C). The main olfactory bulb (MOB), which lies rostral to the telencephalon, was devoid of DAB reaction product, confirming the specificity of the HRP labeling for the vomeronasal pathway.

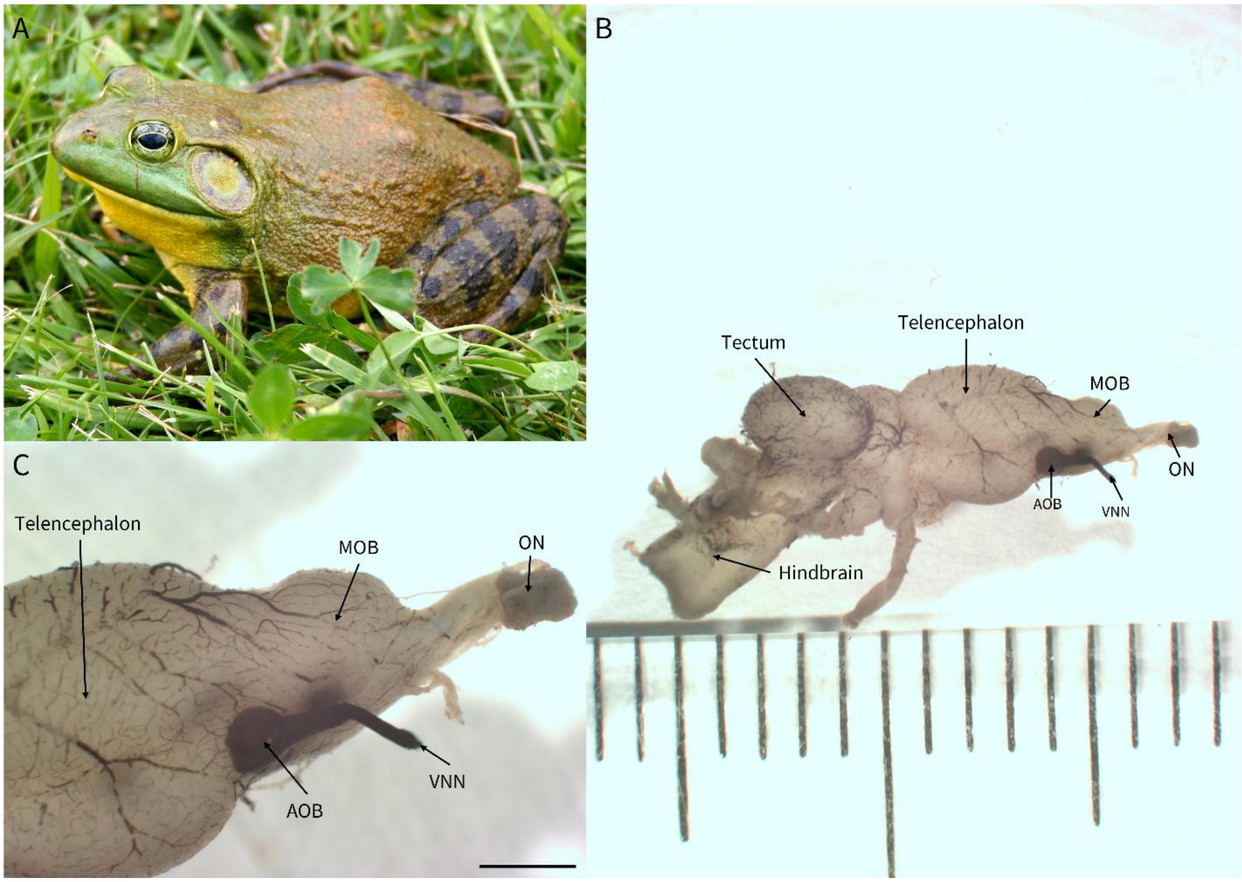

Figure 3. Gross morphology of *Lithobates catesbeiana* and HRP anterograde labeling of the vomeronasal nerve. (A) Adult male *Lithobates catesbeiana*. The tympanum (round disc posterior to the eye) is larger than the eye, a feature characteristic of males. Photo: Carl D. Howe, Wikimedia Commons (File: North-American-bullfrog1.jpg), CC BY-SA 2.5. **(B)** Lateral view of an isolated *L. catesbeiana* brain following HRP application onto the cut stump of the vomeronasal nerve and DAB reaction. Rostral at right. Dark DAB reaction product is tightly localized to the vomeronasal nerve (VNN) and the accessory olfactory bulb (AOB), reflecting anterograde HRP transport. Main olfactory bulb (MOB) and olfactory nerve (ON) are also indicated. Ruler tick spacing = 1 mm. **(C)** Higher magnification lateral view of the rostral brain, rostral at right. The main olfactory bulb (MOB) forms the large pale rostral face of the telencephalon. The AOB is visible on the ventral aspect of the olfactory bulb as a discrete DAB-positive deposit. The incoming VNN is visible as a dark fiber tract projecting into the AOB. Scale bar = 1 mm.

3.2 Histology of the Vomeronasal Nerve

Cross-sectional light microscopic examination of the combined vomeronasal and olfactory nerve revealed two anatomically distinct subdivisions within a shared epineurial sheath (Fig. 4A). The olfactory nerve (ON) comprised the large fasciculated mass occupying the majority of the nerve cross-section, while the vomeronasal nerve (VNN) formed a distinct crescent-shaped subdivision at the periphery. At the electron microscopic level, the VNN was organized into discrete fascicles separated by perineurial septa (Fig. 4B). Higher magnification examination of individual VNN fascicles revealed a densely packed population of small, round to oval unmyelinated axon profiles organized into subfascicles (Fig. 4C). A small number of larger, electron-dense profiles of irregular morphology were observed scattered throughout the fascicles; these are interpreted as fixation or processing artifacts.

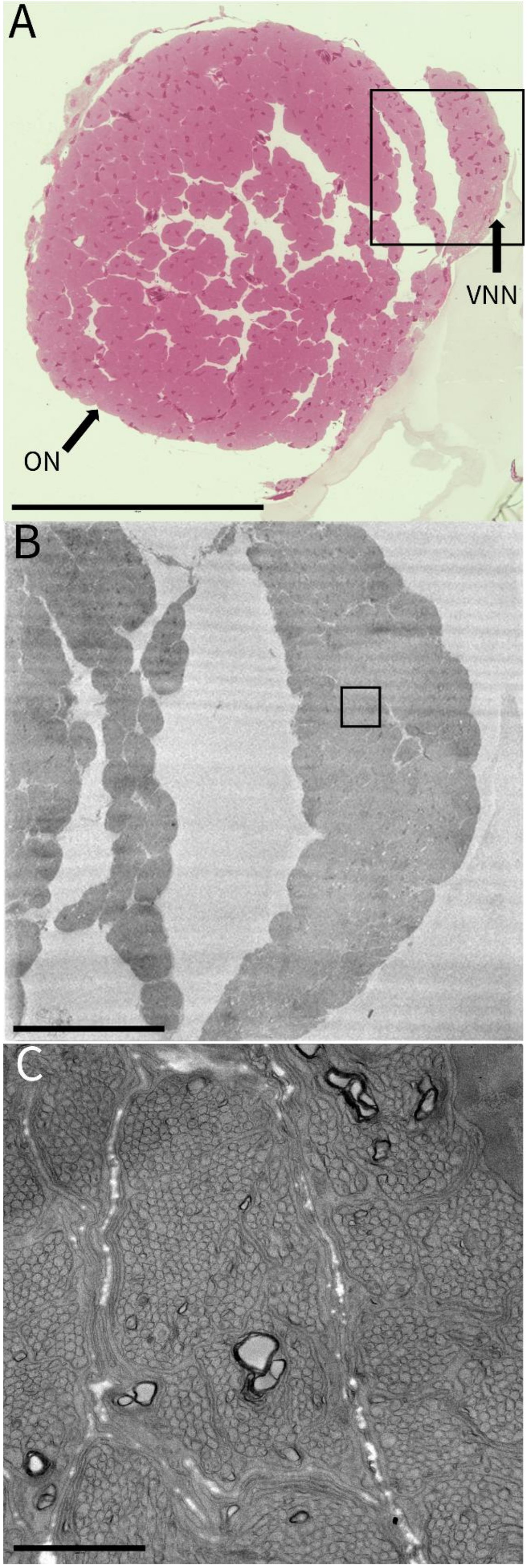
A
VNN
ON
B
C

Figure 4. Histology of the vomeronasal nerve of *Lithobates catesbeiana*. (A) Low magnification light micrograph of a resin-embedded semithin cross-section through the combined vomeronasal and olfactory nerve, stained with azure B–basic fuchsin. The olfactory nerve (ON) comprises the large fasciculated mass occupying the majority of the nerve cross-section. The vomeronasal nerve (VNN) forms a distinct crescent-shaped subdivision at the periphery. Box indicates the region shown in (B). Scale bar = 250 µm. **(B)** Low magnification transmission electron micrograph of the region indicated in (A), showing the fascicular organization of the VNN. Discrete fascicles are separated by perineurial septa. Box indicates the region shown in (C). Scale bar = 30 µm. **(C)** Higher magnification transmission electron micrograph of a VNN fascicle, showing densely packed unmyelinated axon profiles. Connective tissue septa delineate individual subfascicles. Larger electron-dense profiles of irregular morphology are interpreted as fixation artifacts. Scale bar = 2 µm.

3.3 Ultrastructural Comparison of VNN Fascicle Types and Axon Diameter Analysis

Transmission electron microscopy of the VNN revealed morphologically distinct fascicle types within the nerve. Type A fascicles contained a densely packed, morphologically uniform population of small, round to oval unmyelinated axon profiles (Fig. 5A, B); individual subfascicles are indicated by yellow outlines in Fig. 5A. Type B fascicles contained a similar dominant population of small, unmyelinated axons but additionally harboured a sparse subpopulation of substantially larger profiles (Fig. 5C, D). Quantitative measurement of the minimum diameters of axons with circular profiles confirmed this distinction. In a Type A fascicle (n = 609 axons), diameters followed a unimodal distribution with a peak in the 103–154 nm range and a maximum of approximately 216 nm (Fig. 5E). In a Type B fascicle (n = 519 axons), the dominant peak was similarly located at 103–154 nm but a sparse population of large-diameter profiles extending to approximately 681 nm was present, producing a distribution with a pronounced tail absent from Type A fascicles (Fig. 5E). The relationship between Type A and Type B fascicle populations and the bimodal compound action potential profile previously recorded from the VNN of *L. catesbeiana* (K. Delaney, unpublished data) warrants further investigation.

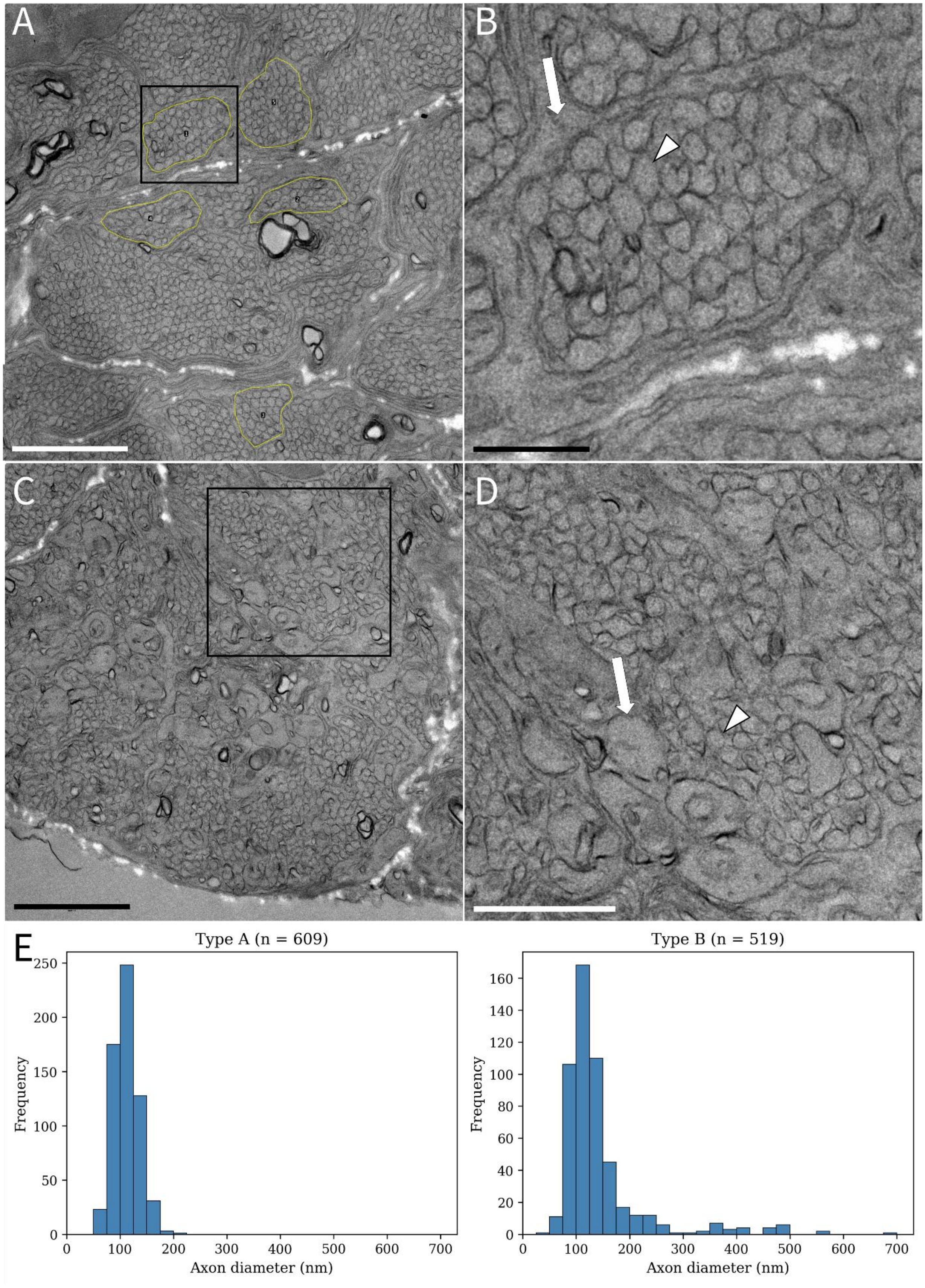
A
B
C
D
E
Type A (n = 609)
Frequency
250
200
150
100
50
0
0
100
200
300
400
500
600
700
Axon diameter (nm)
Type B (n = 519)
Frequency
160
140
120
100
80
60
40
20
0
0
100
200
300
400
500
600
700
Axon diameter (nm)

Figure 5. Ultrastructural comparison of vomeronasal nerve fascicle types in *Lithobates catesbeiana* and axon diameter analysis. (A) Low magnification transmission electron micrograph of a Type A VNN fascicle, showing a densely packed, morphologically uniform population of small unmyelinated axon profiles. Yellow outlines indicate individual subfascicles. Box indicates region shown in (B). Scale bar = 2 µm. **(B)** Higher magnification view of the Type A fascicle shown in (A), showing the uniform small axon profile population in detail. Arrowhead indicates a small axon profile. Arrow indicates a connective tissue septum between subfascicles. Scale bar = 500 nm. **(C)** Low magnification transmission electron micrograph of a Type B VNN fascicle, showing a mixed population of small axon profiles alongside a sparse subpopulation of substantially larger profiles. Box indicates region shown in (D). Scale bar = 2 µm. **(D)** Higher magnification view of the Type B fascicle shown in (C), showing both the dominant small axon population and the sparse large-diameter profiles. Arrowhead indicates a small axon profile. Arrow indicates a large-diameter profile. Scale bar = 1 µm. **(E)** Histograms of axon minimum diameter distributions for Type A (left, n = 609) and Type B (right, n = 519) fascicles. The Type A fascicle shows a unimodal distribution with a peak in the 103–154 nm range. The Type B fascicle shows a similar dominant peak but with a pronounced tail of large-diameter profiles extending to approximately 681 nm, absent from the Type A distribution.

3.4 Histology of the Accessory Olfactory Bulb

To characterize the gross organization and laminar architecture of the AOB, resin-embedded semithin sections were prepared from vibratome-sectioned tissue and examined by light microscopy. HRP application to the cut stump of the vomeronasal nerve and subsequent DAB reaction confirmed the location of the AOB as a discrete extension of the lateral-ventral aspect of the olfactory bulb in both whole brain preparations and vibratome sections (Fig. 6A, B). Semithin sections stained with azure B–basic fuchsin revealed a distinctly laminated structure spanning the full depth from the superficial to the ventricular surface (Fig. 6C, D). Proceeding inward from the superficial surface, a glomerular layer was identifiable by its darkly staining neuropil punctuated by sparse nuclei (Fig. 6E), consistent with a sparse periglomerular cell population relative to the densely populated glomerular layers described in mammals (Mucignat-Caretta, 2010). Deep to the glomerular layer, a mitral cell layer was identifiable by position, giving way inward to a granule cell layer of visibly greater nuclear density approaching the ventricular surface. Corresponding light and electron microscopy of the glomerular region facilitated identification of glomeruli by TEM (Fig. 6F). High magnification TEM of the glomerular neuropil revealed densely packed synaptic terminals surrounded by streaming dendritic profiles (Fig. 6G), consistent with the neuropil organization characteristic of olfactory glomeruli (Burton et al., 1990).

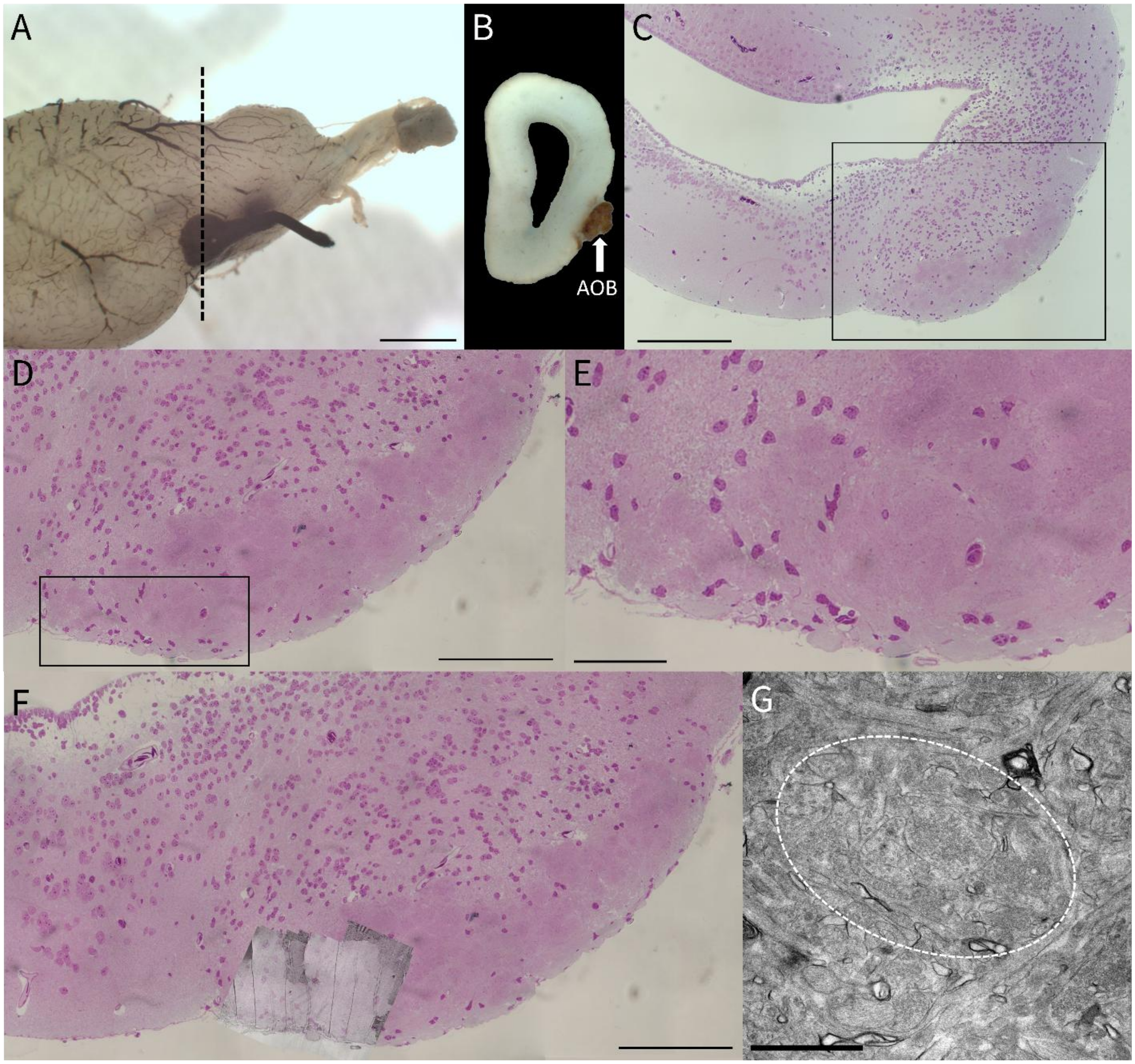

Figure 6. Histology of the accessory olfactory bulb of *Lithobates catesbeiana*. (A) Lateral view of an isolated brain following HRP application to the cut stump of the vomeronasal nerve and DAB reaction. Dashed line indicates the approximate plane of sectioning shown in (B). Scale bar = 1 mm. **(B)** Vibratome section through the olfactory bulb region following HRP application and DAB reaction. The AOB is identifiable as a discrete brown DAB-positive deposit on the ventral aspect of the section. **(C)** Low magnification light micrograph of a resin-embedded semithin section through the AOB, stained with azure B–basic fuchsin. Box indicates the region shown in (D). Scale bar = 500 µm. **(D)** Higher magnification view of a portion of the boxed region in (C), showing the full depth of the AOB from the superficial surface to the ventricular surface. Distinct laminae are visible: a glomerular layer characterized by sparse nuclear density at the superficial surface, a densely cellular mitral cell layer, and a granule cell layer approaching the ventricular surface. Box indicates the region shown in (E). Scale bar = 250 µm. **(E)** Higher magnification view of the boxed region in (D), showing the glomerular layer at the superficial surface. The sparse nuclear density of this zone is consistent with a reduced periglomerular cell population relative to the mitral cell layer visible deeper in (D). Scale bar = 100 µm. **(F)** Corresponding light and electron microscopy of the superficial glomerular layer. Scale bar = 250 µm. **(G)** High magnification transmission electron micrograph of glomerular neuropil, showing synaptic terminals and streaming dendritic profiles. Scale bar = 3 µm.

3.5 Ultrastructure of the Accessory Olfactory Bulb Glomerular Layer

At higher magnification, the glomerular neuropil revealed densely packed synaptic terminals and dendritic profiles in multiple orientations (Fig. 7A). Dendritic profiles were identifiable by their microtubule content and appeared in cross-section, oblique, and longitudinal orientations throughout the neuropil (Fig. 7C, D). These orientations are illustrated schematically in Fig. 7B. Synaptic regions were identified by the presence of synaptic vesicles and postsynaptic densities. Within the glomerular neuropil, several ultrastructural features of interest were identified (Fig. 7E). A likely dendrodendritic synapse was observed, characterized by two adjacent dendritic profiles with synaptic vesicles localized to their respective membranes at the point of contact. A likely gap junction was also seen, characterized by a reduced intercellular space between two profiles and dark striations running perpendicular to their membranes at the point of contact that may be indicative of connexon channels. Additionally, a large vesicular profile with an electron-dense core was observed among smaller clear-core vesicles in one terminal, morphologically consistent with a dense-core vesicle. As this observation was made in non-HRP-reacted tissue, the identity of the containing terminal cannot be confirmed.

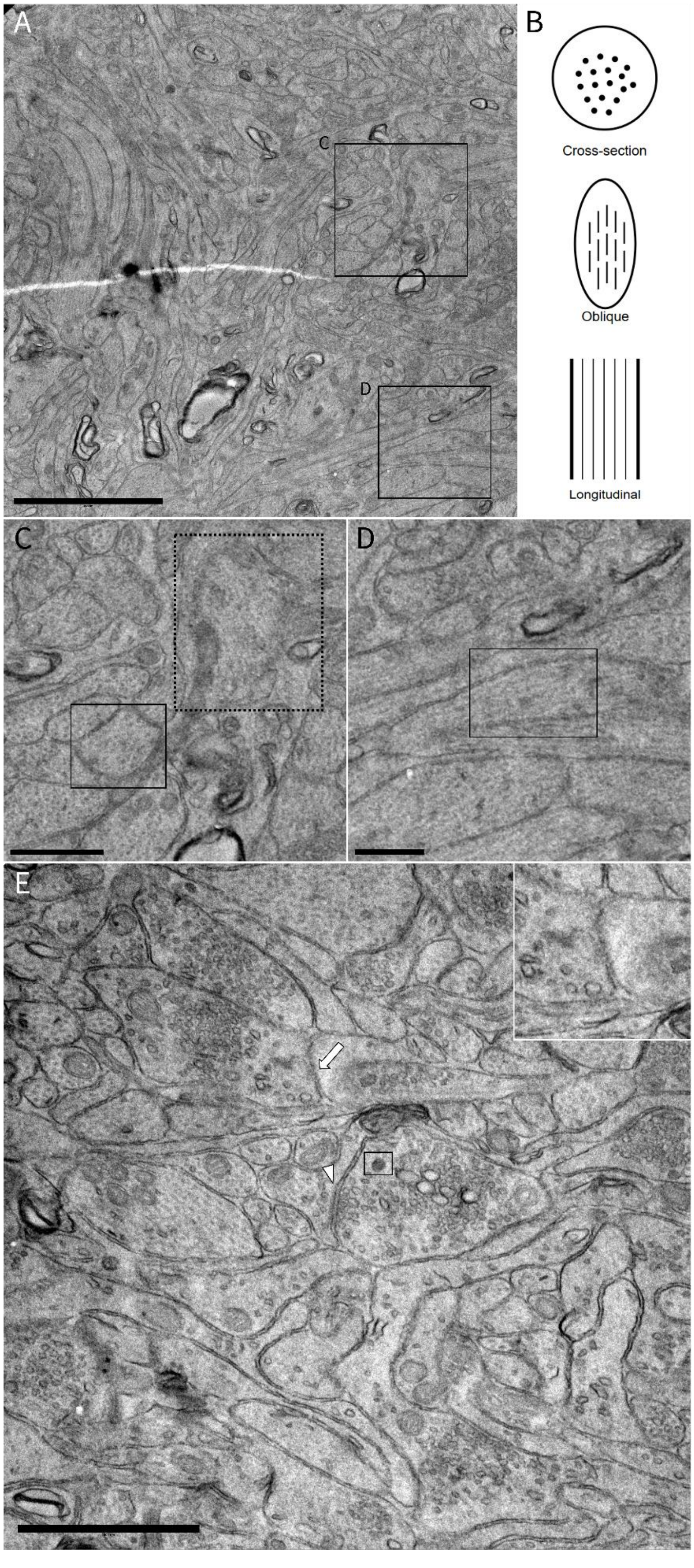
A
C
D
B
Cross-section
Oblique
Longitudinal
C
D
E

Figure 7. Ultrastructural organization of the accessory olfactory bulb glomerular layer of *Lithobates catesbeiana*. (A) Transmission electron micrograph of AOB glomerular neuropil, showing the characteristic organization of a glomerulus: densely packed synaptic terminals interdigitating with dendritic profiles in multiple orientations. Boxes indicate regions shown in (C) and (D). Scale bar = 2 μm. **(B)** Schematic diagram illustrating the three orientations in which dendrites appear in cross-sectional TEM preparations of glomerular neuropil: cross-section, oblique, and longitudinal. **(C)** Higher magnification inset from (A) showing cross-sectioned and obliquely cut dendritic profiles, identifiable by their circular to oval morphology and microtubule content. Dotted box indicates an obliquely cut dendrite. Solid box indicates a cross-sectioned dendrite. Scale bar = 750 nm. **(D)** Higher magnification inset from (A) showing longitudinally cut dendritic profiles, identifiable by their elongated morphology and parallel microtubule arrays. Box indicates a longitudinally cut dendrite. Scale bar = 500 nm. **(E)** Higher magnification transmission electron micrograph showing notable synaptic features observed in the AOB glomerular layer. Arrowhead indicates a likely dendrodendritic synapse. Arrow indicates a likely gap junction, also inset in top right. Box indicates a large vesicular profile with an electron-dense core morphologically consistent with a dense-core vesicle; terminal identity is unknown as this image was acquired from non-HRP-reacted tissue. Scale bar = 1 μm.

3.6 DAB Reaction Products in AOB Presynaptic Compartments

To identify the ultrastructural features of VNN afferent terminals specifically, TEM was performed on HRP-reacted tissue in which DAB reaction product confirmed terminal identity. Electron-dense DAB-labeled terminals were readily identifiable within the glomerular neuropil, distributed among unlabeled neurite profiles (Fig. 8A, C). Within DAB-labeled terminals, vesicle populations could be resolved through the precipitate. In two labeled terminals, large vesicular profiles with electron-dense cores were observed among the more abundant smaller vesicles, morphologically consistent with dense-core vesicles (Fig. 8B, D). Higher magnification views of these profiles revealed an electron-dense core surrounded by a pale halo (Fig. 8B, D insets), a morphology characteristic of dense-core vesicles (Burton, 1990). These observations suggest that DCVs may be present in VNN afferent terminals in *L. catesbeiana*, though conclusive identification is limited by the small number of profiles examined and the partial obscuring of vesicle morphology by DAB reaction product.

In addition, a mitochondrion was observed spanning the interface between two adjacent DAB-labeled terminals (Fig. 8E, F). The two terminals were in close proximity but not fully apposed, with extracellular space visible between them except at the point of mitochondrial crossing. The majority of the mitochondrion was contained within the two flanking terminals, with only a small portion traversing the intervening extracellular space, suggesting the organelle was distributed across both terminals simultaneously. At higher magnification, internal membrane folding consistent with cristae was visible within the structure (Fig. 8F). This observation is consistent with intercellular mitochondrial transfer, a phenomenon documented in other neural contexts including between glia and neurons (Hayakawa et al., 2016; Chakraborty et al., 2023), though transfer specifically between presynaptic terminals has not previously been reported. Conclusive identification and mechanistic interpretation of this finding require further investigation.

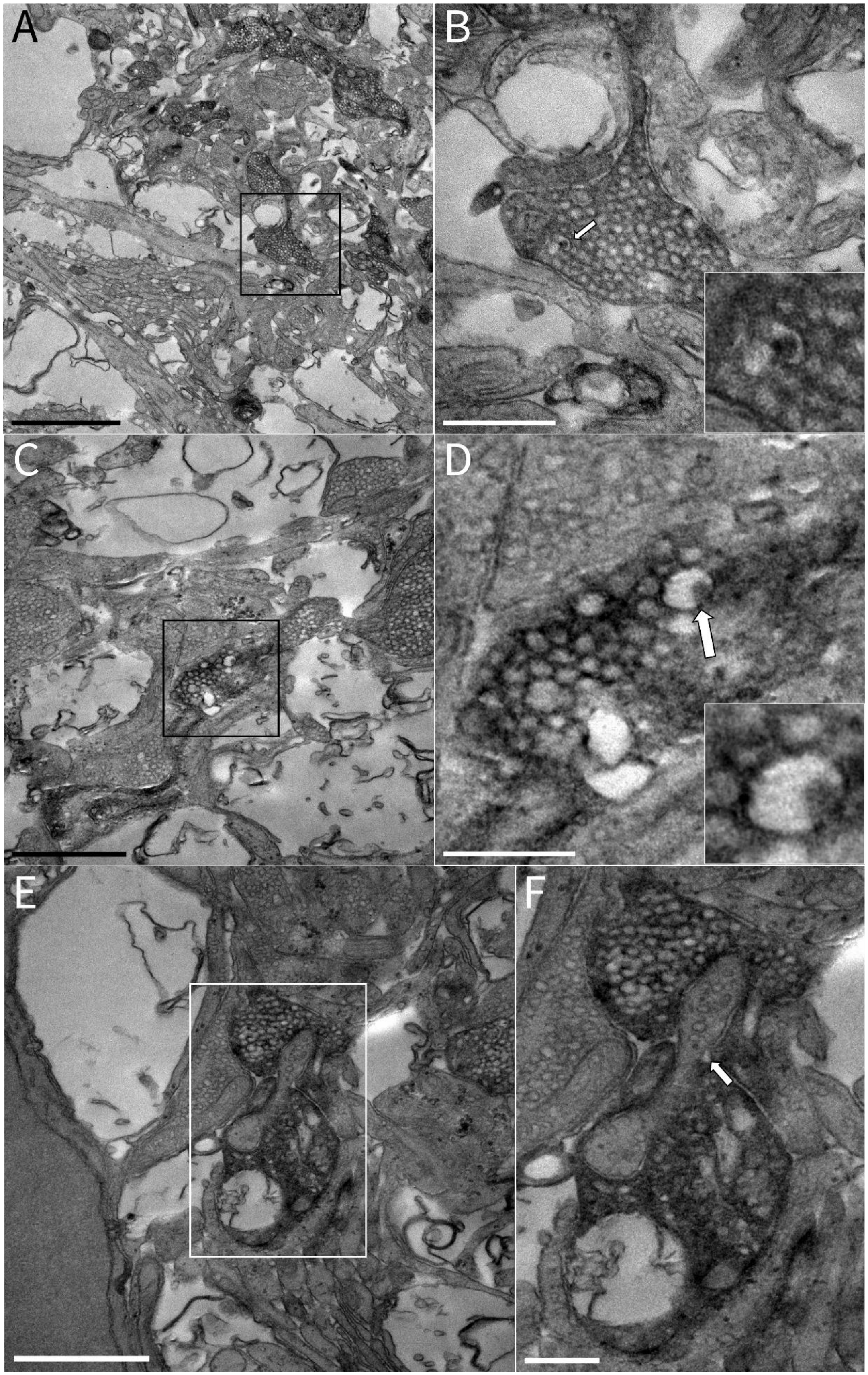
A
B
C
D
E
F

Figure 8. DAB reaction products in presynaptic compartments of the accessory olfactory bulb from HRP-loaded vomeronasal nerves of *Lithobates catesbeiana*. (A) Transmission electron micrograph of DAB-labeled terminals in the AOB glomerular layer. Multiple electron-dense HRP-DAB reaction product-filled terminals are visible among unlabeled dendritic profiles, confirming effective anterograde labeling of VNN afferent terminals. Box indicates the region shown in (B). Scale bar = 2 µm. **(B)** Higher magnification view of a DAB-labeled terminal. Arrow indicates a large vesicular profile with an electron-dense core morphologically consistent with a dense-core vesicle (DCV). Scale bar = 500 nm. Inset shows the indicated profile at higher magnification. **(C)** Transmission electron micrograph showing DAB-labeled terminals at intermediate magnification, illustrating the distribution of labeled presynaptic profiles within the glomerular neuropil. Box indicates the region shown in (D). Scale bar = 1 µm. **(D)** High magnification view of a DAB-labeled terminal showing a large vesicular profile with electron-dense core (arrow), morphologically consistent with a dense-core vesicle. Scale bar = 300 nm. Inset shows the indicated profile at higher magnification. **(E)** Transmission electron micrograph showing two adjacent DAB-labeled terminals connected by a structure morphologically consistent with a mitochondrion extending between them, suggestive of intercellular mitochondrial transfer. Box indicates region shown in (F). Scale bar = 1 µm. **(F)** Higher magnification view of the region indicated in (E). Arrow indicates the point at which the likely mitochondrion extends across the extracellular space. Scale bar = 300 nm.

Discussion

4.1 Laminar Organization of the Accessory Olfactory Bulb

This study builds on Burton's (1990) previous ultrastructural work on the *L. catesbeiana* AOB, adding semithin section histology of the laminar organization, HRP-DAB tracing to confirm VNN terminal identity, and corresponding light and electron microscopy of the incoming VNN fascicles and a superficial region of the glomerular layer. Azure B–basic fuchsin staining of semithin sections revealed clear laminar organization that is consistent with prior descriptions of the frog AOB (Kemali & Guglielmotti, 1987; Burton et al., 1990). From the superficial surface inward, a glomerular layer, mitral cell layer, and granule cell layer were all identifiable, broadly matching the layered organization that has been described in the rodent AOB (Mucignat-Caretta, 2010).

One notable feature of the *L. catesbeiana* AOB was the sparse nuclear density of the glomerular layer relative to the mitral cell layer, indicating a reduced periglomerular cell population compared to previous studies in rodents. In the rodent MOB and AOB, the glomerular layer contains a dense population of periglomerular interneurons that provide local inhibitory and modulatory control over afferent input (Mucignat-Caretta, 2010). The apparent sparse periglomerular cell population in the frog AOB is consistent with Burton's description of the bullfrog AOB as less organized than the primary olfactory lobe, with reduced numbers of tufted and periglomerular cells relative to mammals (Burton, 1990). This reduction in periglomerular cell complement is a genuine and substantive feature of frog AOB organization, representing a meaningful departure from the mammalian pattern and consistent with the broader characterization of the frog AOB as a less elaborated structure.

The mitral cell layer was clearly defined as a densely cellular zone, with large mitral cell somata identifiable at higher magnification, consistent with Burton's description of mitral cells as the largest neurons in the AOB neuropil (Burton, 1990). This organization is consistent with Burton's observation that mitral cells in the frog AOB are scattered throughout the neuropil rather than confined to a discrete layer, with no clearly bounded external plexiform layer separating glomerular and mitral cell zones. Corresponding light and electron microscopy confirmed the transition from incoming VNN fascicles into the superficial glomerular layer, establishing the spatial relationship between the afferent nerve and its termination zone and providing a structural framework for interpreting the TEM observations that follow.

4.2 Organization and Ultrastructure of the Vomeronasal Nerve

Cross-sectional examination of the combined vomeronasal and olfactory nerve revealed a morphologically distinct crescent-shaped subdivision at the periphery of the nerve, enclosed within a shared epineurial sheath alongside the substantially larger olfactory nerve, consistent with the position of the VNN as described by Burton et al. (1990), who described the VNN as a discrete nerve running along the lateral and ventral aspect of the olfactory nerve, from which it cannot be distinguished by superficial examination but which can be followed by careful dissection to where it terminates in the AOB.

At the electron microscopic level, the VNN was organized into discrete fascicles and subfascicles separated by perineurial septa, each containing a densely packed population of small, round to oval unmyelinated axon profiles. This subfascicular organization was not seen in the accompanying olfactory nerve. The unmyelinated character of the VSN axons is consistent with Burton et al. (1990), who described VSN axons as ultrastructurally indistinguishable from primary olfactory axons, both being small and unmyelinated. The fascicular organization observed here extends Burton's description by identifying a subdivision of the nerve into fascicle types with distinct axon diameter distributions.

Two morphologically distinct fascicle types were identified in the VNN, here designated Type A and Type B. Type A fascicles contained a morphologically uniform population of small axon profiles with a unimodal diameter distribution peaking in the 103–154 nm range. Type B fascicles contained a similar dominant population of small axons but additionally harboured a sparse subpopulation of substantially larger profiles, producing a roughly bimodal distribution with a pronounced tail extending to approximately 681 nm. This distinction was not described by Burton et al. (1990), whose axon counts and neurofilament analyses treated the VNN as a uniform population and therefore represents a novel observation from the present study.

Preliminary observations suggest that Type B fascicles may be associated with a greater abundance of dark-bordered profiles that may be interpreted as fixation or processing artifacts. The absence of microtubules in the dark-bordered profiles, which are a consistent feature of axon profiles in this preparation, argues against their identification as axons, though partial myelination cannot be entirely excluded. While the large-diameter axon profiles and the artifact-like profiles are morphologically distinct, their co-occurrence raises the possibility that Type B fascicles may be more susceptible to fixation or processing damage than Type A fascicles, whether due to differences in axon composition, connective tissue organization, or some other property. This does not rule out the large-diameter profiles as a genuine axon subpopulation but introduces a degree of uncertainty regarding the fidelity of preservation in this fascicle type that should be considered when interpreting the diameter distribution data.

The functional significance of the Type A/Type B distinction is unclear but potentially relates to the bimodal compound action potential profile recorded from the *L. catesbeiana* VNN in the Delaney laboratory (K. Delaney, unpublished data). It is well established that axon conduction velocity scales with axon diameter in unmyelinated fibers, such that a bimodal diameter distribution would predict two peaks in the conduction velocity profile (Augustine et al., 2023). The large-diameter profiles in Type B fascicles are candidates for a faster-conducting axon subpopulation that could contribute to the second compound action potential peak. They could represent fixation or processing artifacts, though their consistent morphology and presence specifically in Type B fascicles argues against this interpretation. Resolving this question would require a larger sample size across multiple animals and nerve levels, serial section reconstruction, or immunolabeling to determine whether the large-diameter profiles share molecular markers with the small unmyelinated VSN axons or represent a distinct cell type.

It is also notable that not all fascicles examined contained the large-diameter profile subpopulation, raising the possibility that Type A and Type B fascicles may represent anatomically segregated subpopulations within the nerve rather than a random mixture. Whether this segregation is consistent across animals and reflects a genuine organizational principle of the *L. catesbeiana* VNN warrants systematic investigation in future work.

4.3 Ultrastructure of the AOB Glomerular Layer: Dendrodendritic Synapses and Gap Junctions

Transmission electron microscopy of the AOB glomerular layer revealed densely packed, roughly ovoid cores of synaptic terminals surrounded by dendritic profiles sectioned in multiple orientations. This organization is consistent with Burton's description of AOB glomeruli in the adult bullfrog, which he characterized as compact structures containing abundant axon terminals and mitral cell dendrites with numerous synaptic contacts (Burton, 1990). The present study confirms this description by identifying the dendritic profiles surrounding the synaptic regions in cross-sectional, oblique, and longitudinal orientations within the glomerular neuropil, reflecting the complex three-dimensional branching pattern of mitral cell apical dendrites within glomeruli.

Within the glomerular neuropil, a likely dendrodendritic synapse was identified, characterized by two adjacent dendritic profiles with synaptic vesicles clustered at the membrane on at least one side and a visible postsynaptic density. Dendrodendritic synapses are a well-established feature of the mammalian olfactory bulb, where reciprocal contacts between mitral cell lateral dendrites and granule cell spines in the external plexiform layer of the MOB provide recurrent and lateral inhibition (Bartel et al., 2015). Burton (1990) documented dendrodendritic synapses extensively in the frog AOB, especially in the periglomerular neuropil and deeper layers between mitral and presumed granule cell dendrites. However, Burton does not appear to report dendrodendritic synapses within the glomerular layer itself. Therefore, the observation of a likely dendrodendritic synapse within the glomerular neuropil is potentially novel relative to Burton's description and if confirmed, would suggest that dendrodendritic signaling in the frog AOB is not limited to the periglomerular and deeper neuropil as Burton implies.

A likely gap junction was also identified in the glomerular neuropil, consisting of a close membrane apposition between two adjacent profiles with a markedly reduced intercellular space. Gap junctions between mitral cell dendrites have been documented in the mammalian olfactory bulb, where they are proposed to contribute to synchronization of mitral cell activity within glomeruli (Christie et al., 2005; Bourne & Schoppa, 2017; Maher et al., 2009). Burton (1990) does not report gap junctions in the frog AOB and to our knowledge no prior ultrastructural study has documented gap junctions in the anuran AOB. The present observation is therefore consistent with a feature of glomerular circuit organization that may be conserved between frogs and mammals, though conclusive identification would require immunohistochemical or freezefracture analysis to resolve the characteristic pentalaminar membrane structure of a true gap junction, in which two adjacent membranes enclose a narrow extracellular space (Christie et al., 2005).

It should be noted that both the likely dendrodendritic synapse and the likely gap junction were observed in non-HRP-reacted tissue, meaning the identities of the profiles involved cannot be confirmed. The dendritic identity of the profiles in both cases was inferred from microtubule content and morphology, consistent with established criteria for identifying dendritic profiles in TEM preparations of olfactory neuropil (Burton, 1990). Confirmation of these observations in additional tissue samples and ideally in HRP-reacted tissue where terminal identity can be established would strengthen the interpretations made here.

4.4 Dense-Core Vesicles in VNN Afferent Terminals and Implications for Activity-Dependent Enhancement

A central aim of the present study was to determine whether dense-core vesicles are present in VNN afferent terminals in the AOB of *L. catesbeiana*, as a prerequisite for evaluating the hypothesis that neuropeptide co-release from DCVs contributes to the presynaptic mechanism underlying activity-dependent enhancement. Two observations bearing on this question were made; however, for the reasons discussed below, neither provides sufficient evidence to confirm the presence of DCVs in VNN afferent terminals.

First, in non-HRP-reacted tissue, large vesicles with electron-dense cores were observed among smaller clear-core vesicles in multiple terminals within the glomerular neuropil across several images (Fig. 7E; see also Appendix B), morphologically consistent with dense-core vesicles. However, as this observation was made in the absence of HRP-DAB labeling, the identity of the containing terminal, whether a VNN afferent terminal, a periglomerular cell terminal, or another profile, cannot be confirmed. This observation therefore cannot be attributed to VNN afferents with certainty.

Second, large vesicular profiles with electron-dense cores were observed in DAB-labeled terminals in HRP-reacted tissue, with DAB reaction product confirming the identity of these terminals as VNN afferents. Higher magnification views revealed an electron-dense core surrounded by a pale halo, a morphology that has been described for dense-core vesicles (Burton, 1990). However, given the small number of profiles observed, the partial obscuring of fine morphology by DAB precipitate, and the difficulty of distinguishing DCVs from other large vesicular structures under these imaging conditions, this observation cannot be taken as confirmation that DCVs are present in VNN afferent terminals in *L. catesbeiana*.

Burton (1990) described dense-cored vesicles in VNN axon terminals in the bullfrog AOB glomerular layer alongside the more abundant lucent vesicles, and also documented DCVs broadly across mitral cell perikarya and pre- and postsynaptic dendrites at dendrodendritic synapses. While the large vesicular profiles observed in the present study are superficially consistent with Burton's description, the present data do not provide sufficient evidence to confirm DCVs in VNN afferent terminals. The observations are limited to a small number of profiles, DAB precipitate reduces morphological resolution, and the profiles cannot be unambiguously distinguished from other large vesicular structures. Systematic quantification across larger datasets with improved tissue preparation would be required before any conclusion regarding DCV presence can be drawn.

The neuropeptide co-release hypothesis that activity-dependent release from DCVs in VNN afferent terminals contributes to ADE was a primary motivation for the present study. Delaney et al. (2009) reported that ADE in the *R. pipiens* AOB is consistent with a presynaptic locus of action and persists under reduced extracellular calcium, making classical residual-calcium-dependent release an unlikely explanation. While neuropeptide co-release from DCVs would be consistent with these properties, the present study does not provide sufficient anatomical evidence to support or refute this hypothesis.

Whether DCVs are present in VNN afferent terminals, what they contain, and whether their release contributes causally to ADE remain open questions. Addressing them would require improved tissue preparation to reduce DAB-related morphological obscuring, systematic quantification across larger datasets, immunolabeling for neuropeptide markers, and ultimately pharmacological manipulation of neuropeptide signaling combined with electrophysiological recording of ADE.

4.5 A Trans-cellular Mitochondrion at the Interface of Adjacent VNN Afferent Terminals

In HRP-reacted tissue, a structure morphologically consistent with a mitochondrion was observed to cross the interface between two adjacent DAB-labeled VNN afferent terminals (Fig. 8E, F). The structure was identifiable by its double membrane boundary and internal membrane folding consistent with cristae, visible at higher magnification. Critically, the majority of the structure was contained within the two adjacent terminals, with only a small portion traversing the intervening extracellular space at the point where the two terminals were in closest proximity. The two terminals were not fully apposed: extracellular space was visible between them except at the point of mitochondrial crossing, suggesting that the structure was distributed across both terminals simultaneously rather than residing entirely within one.

This observation is morphologically consistent with intercellular mitochondrial transfer between presynaptic terminals. Intercellular mitochondrial transfer has been documented in a variety of biological contexts, including between astrocytes and neurons following ischaemic injury in vivo, with ultrastructural confirmation by TEM (Hayakawa et al., 2016) and between microglia and neurons via tunneling nanotube-like structures in cell culture (Chakraborty et al., 2023). While these examples involve glial-to-neuron transfer rather than transfer between presynaptic terminals specifically, they establish that intercellular mitochondrial exchange occurs in neural tissue and provide a framework for interpreting the present observation. However, to our knowledge this phenomenon has not been previously reported in the AOB or in VNN afferent terminals specifically, making this a potentially novel observation for this circuit.

Several interpretive caveats apply. The identification of the structure as a mitochondrion rests on morphological criteria of a double membrane and cristae-like internal folding, which are not definitive in the absence of volumetric or tomographic reconstruction. The single-section nature of the observation means that the three-dimensional relationship between the structure and the two terminals cannot be fully resolved; what appears in two dimensions as a mitochondrion spanning two terminals could in principle represent a mitochondrion within a single terminal that is sectioned at a point where the terminal narrows to near-contact with its neighbour. Serial section reconstruction would be required to establish the three-dimensional geometry of the observation with confidence.

Furthermore, the functional significance of trans-cellular mitochondrial localization at a terminal interface, if confirmed, is not clear. Possibilities include active transfer of mitochondria between terminals via a mechanism analogous to tunneling nanotube-mediated transfer described in other systems, passive localization of a mitochondrion at a site of close membrane apposition, or extrusion of a mitochondrion into the extracellular space following damage, potentially related to the HRP filling procedure in which the nerve was cut and maintained in a pipette overnight prior to fixation. This observation is reported here as a novel and interesting finding that warrants further investigation, including serial section TEM, to characterize the three-dimensional structure of similar instances and to determine whether it represents a reproducible feature of VNN terminal organization in the *L. catesbeiana* AOB.

4.6 Limitations and Future Directions

Several limitations of the present study should be acknowledged. First, the ultrastructural observations reported here are derived from a limited number of tissue preparations from a small number of animals. Key observations including the large vesicular profiles in VNN afferent terminals, the likely dendrodendritic synapse and gap junction in the glomerular layer, and the mitochondrion at the terminal interface are each based on a small number of profiles across a limited image set. While these observations are internally consistent and morphologically well-supported, whether they may be generalized across animals and their frequency within the glomerular layer cannot be assessed from the present data. Systematic quantification across larger image sets and multiple animals will be required to establish whether these features are consistent and abundant components of the *L. catesbeiana* AOB circuit or represent rare or incidental observations.

Second, the quantitative axon diameter analysis of the VNN was performed on a single Type A and a single Type B fascicle, each from a single preparation. While the morphological distinction between fascicle types was clear and the diameter distributions were internally consistent, it is not known whether the Type A/Type B distinction is present consistently across animals, whether the proportion of each fascicle type is consistent, or whether the large-diameter profile subpopulation in Type B fascicles represents a reproducible finding. Expanded sampling across multiple regions in multiple animals and different nerve levels would be necessary to characterize the VNN axon population with confidence.

Third, the present study examined tissue from adult animals only; sex was not systematically recorded across preparations. Burton et al. (1990) demonstrated significant differences in AOB glomerular organization between larval and adult bullfrogs, with tadpole glomeruli less compact and showing fewer synaptic contacts than adult glomeruli. Whether the ultrastructural features documented here, including the terminals with large vesicular profiles, the likely dendrodendritic synapse, and the gap junction, are present in larval tissue and how they relate to the developmental maturation of the circuit are questions that remain open.

Several directions for future investigation follow directly from the present findings. Whether dense-core vesicles are present in VNN afferent terminals remains an open question and a priority for future work. Systematic TEM sampling across larger image sets and multiple animals, combined with immunolabeling for neuropeptide markers, would be required to address it. If DCVs were confirmed, this would provide an anatomical basis for the neuropeptide co-release hypothesis of ADE, which could then be tested directly through pharmacological manipulation of neuropeptide signaling combined with electrophysiological recording.

The fascicle type distinction in the VNN and its potential relationship to the bimodal CAP warrants investigation through expanded axon diameter sampling, immunolabeling for vomeronasal sensory neuron (VSN) subtype markers, and anterograde tracing from morphologically defined VSN subpopulations to determine whether Type A and Type B fascicles represent anatomically segregated projections of distinct VSN populations. Finally, the finding of a single mitochondrion spanning multiple terminals represents an intriguing observation that would benefit from further investigation including serial section TEM to establish its three-dimensional geometry and whether trans-cellular mitochondrial localization is a reproducible feature of VNN terminal organization in this species.

Conclusion

The present study extended the ultrastructural characterization of the *Lithobates catesbeiana* AOB through semithin section histology, transmission electron microscopy, HRP-DAB anterograde tract tracing, and quantitative analysis of VNN axon diameter. The laminar organization of the frog AOB was confirmed, with a glomerular layer and mitral cell layer identified in semithin sections. A notably sparse periglomerular cell population was identified in the glomerular layer, consistent with prior descriptions of the frog AOB as less elaborated than its mammalian counterpart (Burton, 1990); this represents a substantive frog-specific feature of AOB organization. Likely dendrodendritic synapses and gap junctions were identified in the glomerular neuropil, suggesting that circuit features characteristic of the mammalian olfactory bulb may be conserved in the anuran AOB.

Quantitative axon diameter analysis identified two morphologically distinct VNN fascicle types: Type A fascicles with a unimodal small-axon distribution, and Type B fascicles with an additional sparse subpopulation of substantially larger profiles, consistent with the bimodal compound action potential profile previously recorded from this nerve. Large vesicular profiles were observed in HRP-DAB labeled VNN afferent terminals; however, the present data are insufficient to confirm the identity of these profiles as dense-core vesicles, and the anatomical basis for the neuropeptide co-release hypothesis of ADE therefore remains unestablished. Together, these findings advance our understanding of the structural organization of the frog AOB and identify key questions, including the nature of vesicle populations in VNN terminals, that require further investigation.

References

Augustine GJ, Groh JM, Huettel SA, LaMantia AS, White LE, Purves D (2023). Neuroscience, 7th edition. Oxford University Press, New York.

Bartel DL, Rela L, Hsieh L, Greer CA (2015). Dendrodendritic synapses in the mouse olfactory bulb external plexiform layer. J Comp Neurol 523(8):1145–1161.

Bourne JN, Schoppa NE (2017). Three-dimensional synaptic analyses of mitral cell and external tufted cell dendrites in rat olfactory bulb glomeruli. J Comp Neurol 525(3):592–609.

Burton PR (1990). Vomeronasal and olfactory nerves of adult and larval bullfrogs: II. Axon terminations and synaptic contacts in the accessory olfactory bulb. J Comp Neurol 292(4):624–637.

Burton PR, Coogan MM, Borror CA (1990). Vomeronasal and olfactory nerves of adult and larval bullfrogs: I. Axons and the distribution of their glomeruli. J Comp Neurol 292(4):614–623.

Chakraborty R, Nonaka T, Hasegawa M, Zurzolo C (2023). Tunnelling nanotubes between neuronal and microglial cells allow bi-directional transfer of α-Synuclein and mitochondria. Cell Death Dis 14(1):329.

Christie JM, Bark C, Hormuzdi SG, Helbig I, Monyer H, Westbrook GL (2005). Connexin36 mediates spike synchrony in olfactory bulb glomeruli. Neuron 46(5):761–772.

Delaney KR, Qnais EY, Hardy AB (2009). Short-term synaptic plasticity at the main and vomeronasal olfactory receptor to mitral cell synapse in frog. Eur J Neurosci 30(11):2077–2088.

Eisthen HL (1992). Phylogeny of the vomeronasal system and of receptor cell types in the olfactory and vomeronasal epithelia of vertebrates. Microsc Res Tech 23(1):1–21.

Halpern M, Martínez-Marcos A (2003). Structure and function of the vomeronasal system: an update. Prog Neurobiol 70(4):245–318.

Hayakawa K, Esposito E, Wang X, Terasaki Y, Liu Y, Xing C, Ji X, Lo EH (2016). Transfer of mitochondria from astrocytes to neurons after stroke. Nature 535(7613):551–555.

Ishii T, Hirota J, Mombaerts P (2003). Combinatorial coexpression of neural and immune multigene families in mouse vomeronasal sensory neurons. Curr Biol 13(5):394–400.

Jia C, Chen WR, Shepherd GM (1999). Synaptic organization and neurotransmitters in the rat accessory olfactory bulb. J Neurophysiol 81(1):345–355.

Karlupia N, Schalek RL, Wu Y, Meirovitch Y, Wei D, Charney AW, Kopell BH, Lichtman JW (2023). Immersion fixation and staining of multicubic millimeter volumes for electron microscopy–based connectomics of human brain biopsies. Biol Psychiatry 94(4):352–360.

Kemali M, Guglielmotti V (1987). A horseradish peroxidase study of the olfactory system of the frog *Rana esculenta*. J Comp Neurol 263(3):400–417.

Maher BJ, McGinley MJ, Westbrook GL (2009). Experience-dependent maturation of the glomerular microcircuit. Proc Natl Acad Sci USA 106(39):16865–16870.

Morikawa S, Sato A, Ezaki T (2018). A simple, one-step polychromatic staining method for epoxy-embedded semithin tissue sections. Microscopy 67(6):331–344.

Mucignat-Caretta C (2010). The rodent accessory olfactory system. J Comp Physiol A 196(10):749–765.

Mulligan SJ, Davison I, Delaney KR (2001). Mitral cell presynaptic Ca2+ influx and synaptic transmission in frog amygdala. Neuroscience 104(1):137–151.

Quaglino E, Giustetto M, Panzanelli P, Cantino D, Fasolo A, Sassoè-Pognetto M (1999). Immunocytochemical localization of glutamate and γ-aminobutyric acid in the accessory olfactory bulb of the rat. J Comp Neurol 408(1):61–72.

Scalia F, Gallousis G, Roca S (1991). Differential projections of the main and accessory olfactory bulb in the frog. J Comp Neurol 305(3):443–461.

Schindelin J, Arganda-Carreras I, Frise E, Kaynig V, Longair M, Pietzsch T, Preibisch S, Rueden C, Saalfeld S, Schmid B, Tinevez JY, White DJ, Hartenstein V, Eliceiri K, Tomancak P, Cardona A (2012). Fiji: an open-source platform for biological-image analysis. Nat Methods 9(7):676–682.

Toida K, Kosaka K, Heizmann CW, Kosaka T (1998). Chemically defined neuron groups and their subpopulations in the glomerular layer of the rat main olfactory bulb: III. Structural features of calbindin D28K-immunoreactive neurons. J Comp Neurol 392(2):179–198.

Appendix A: Equipment

Figure A1. RMC PowerTome XL ultramicrotome. An RMC PowerTome XL ultramicrotome used for cutting semithin and ultrathin sections from resin-embedded tissue blocks. A diamond knife is visible mounted in the ultramicrotome.

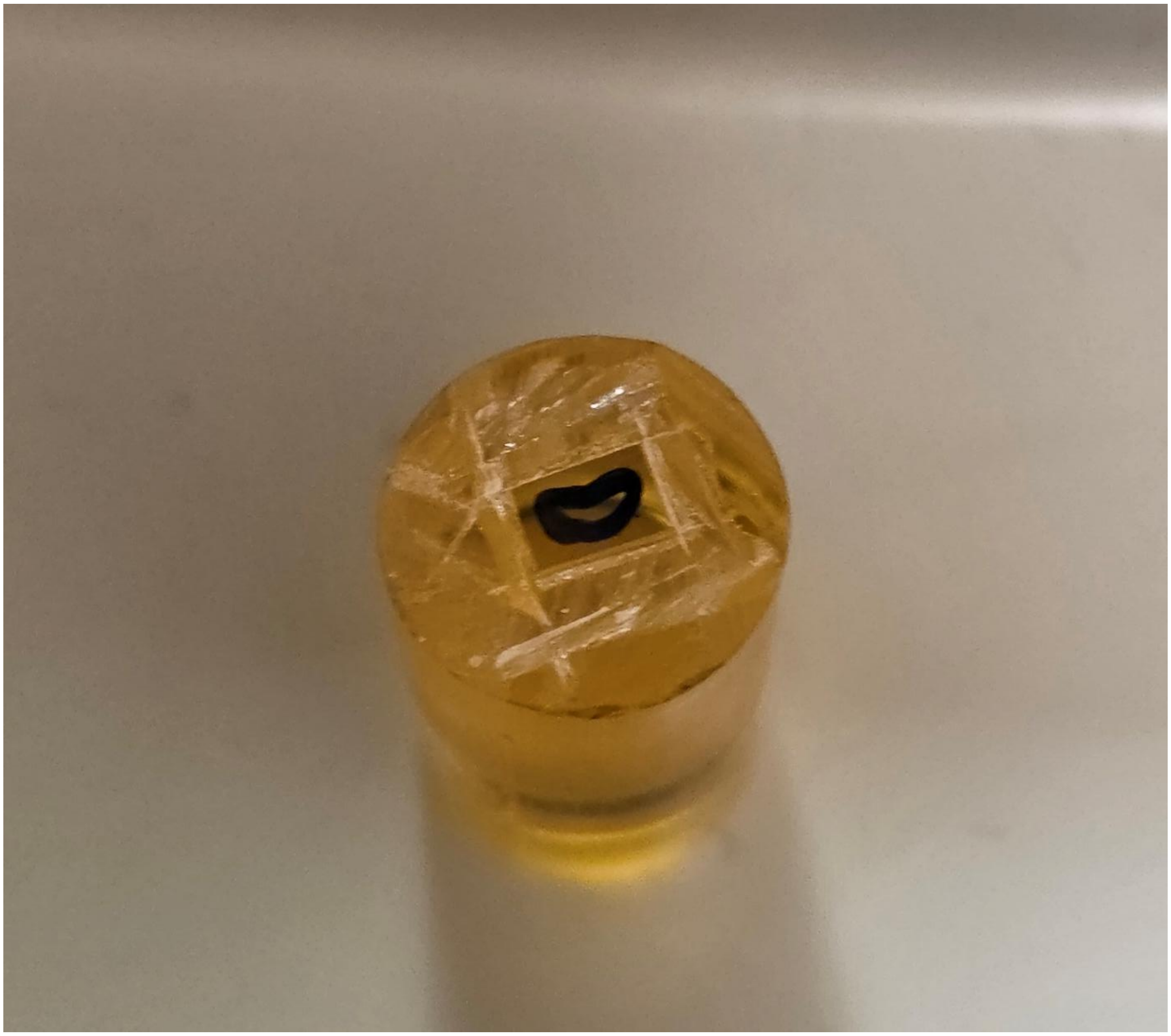

Figure A2. Resin-embedded tissue block prepared for ultrathin sectioning. Resin-embedded tissue block prepared for ultrathin sectioning. The trimmed face of the block contains a cross-section of the telencephalon, visible as a dark crescent-shaped profile within the Epon 812 resin.

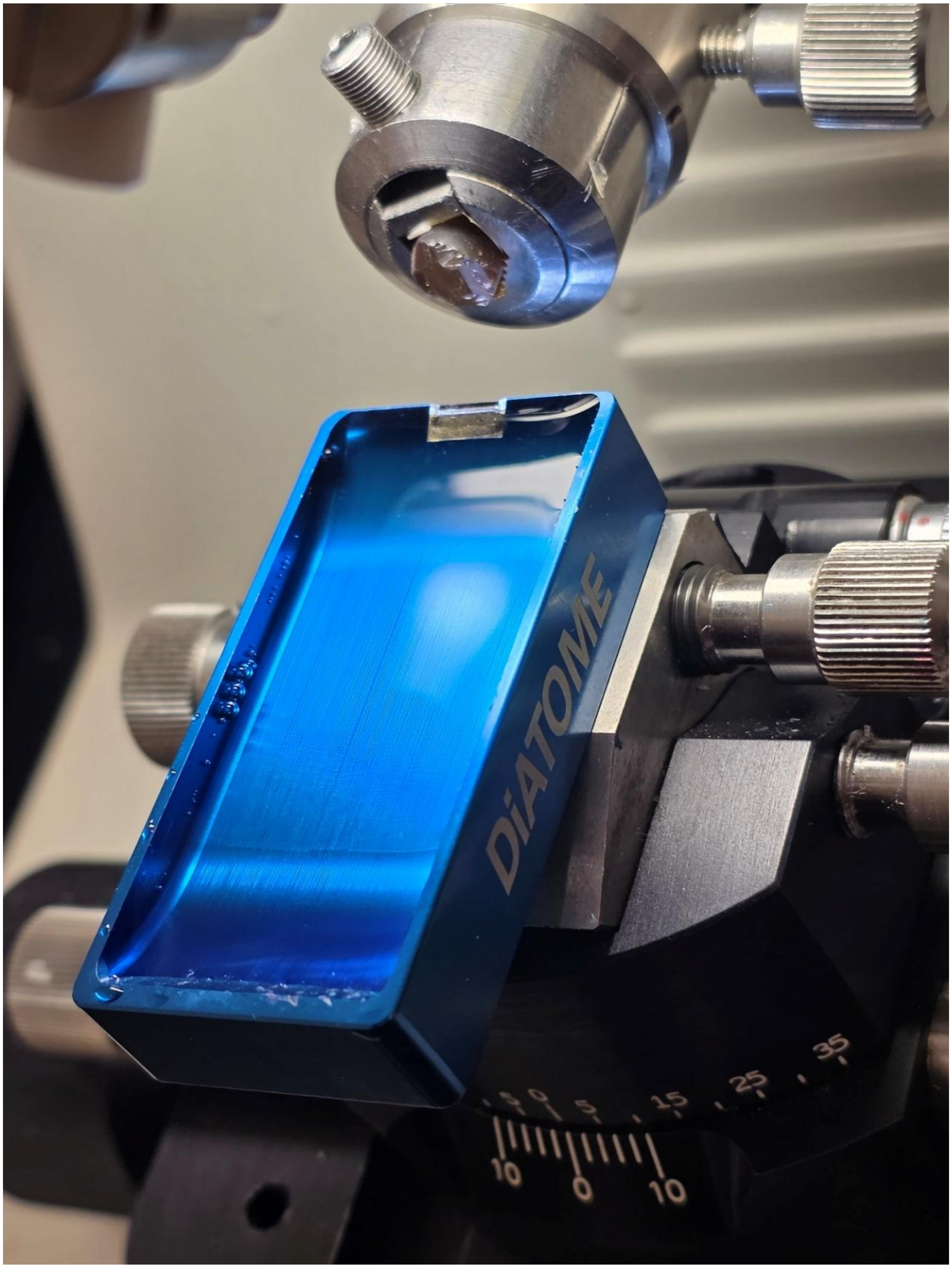

Figure A3. Diatome Histo Jumbo diamond knife mounted in the RMC PowerTome XL ultramicrotome. Diatome Histo Jumbo diamond knife mounted in the RMC PowerTome XL ultramicrotome, filled with water to form a trough for collection of ultrathin sections.

Figure A4. A 200-mesh copper grid bearing an ultrathin section. A 200-mesh copper grid bearing an ultrathin section collected from the water trough of the diamond knife, ready for TEM examination.

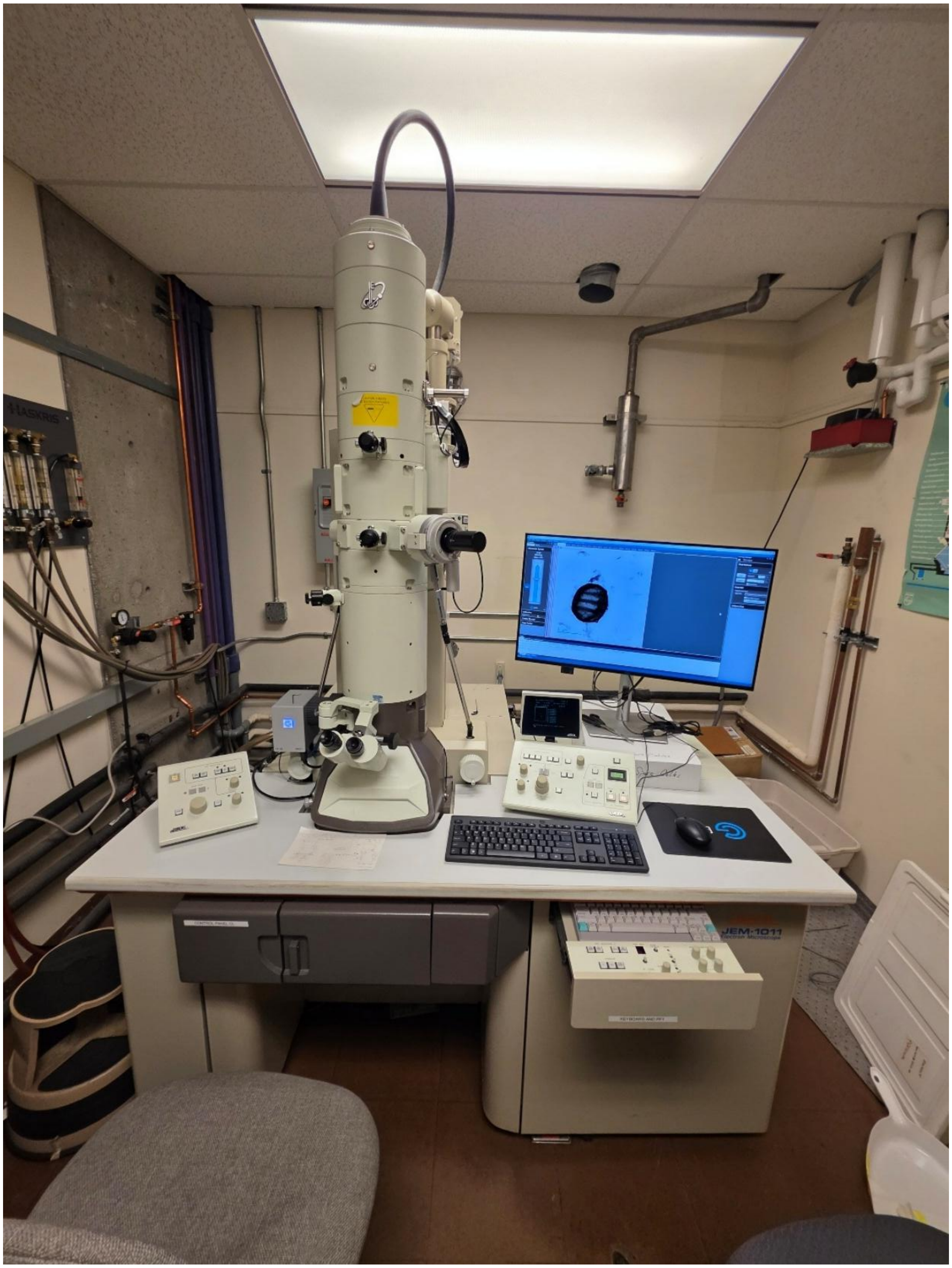

Figure A5. JEOL JEM-1011 transmission electron microscope. JEOL JEM-1011 transmission electron microscope at the University of Victoria Biology Electron Microscopy Facility, used for all ultrastructural imaging in this study.

Appendix B: Additional TEM Images of Large Vesicular Profiles in Terminals

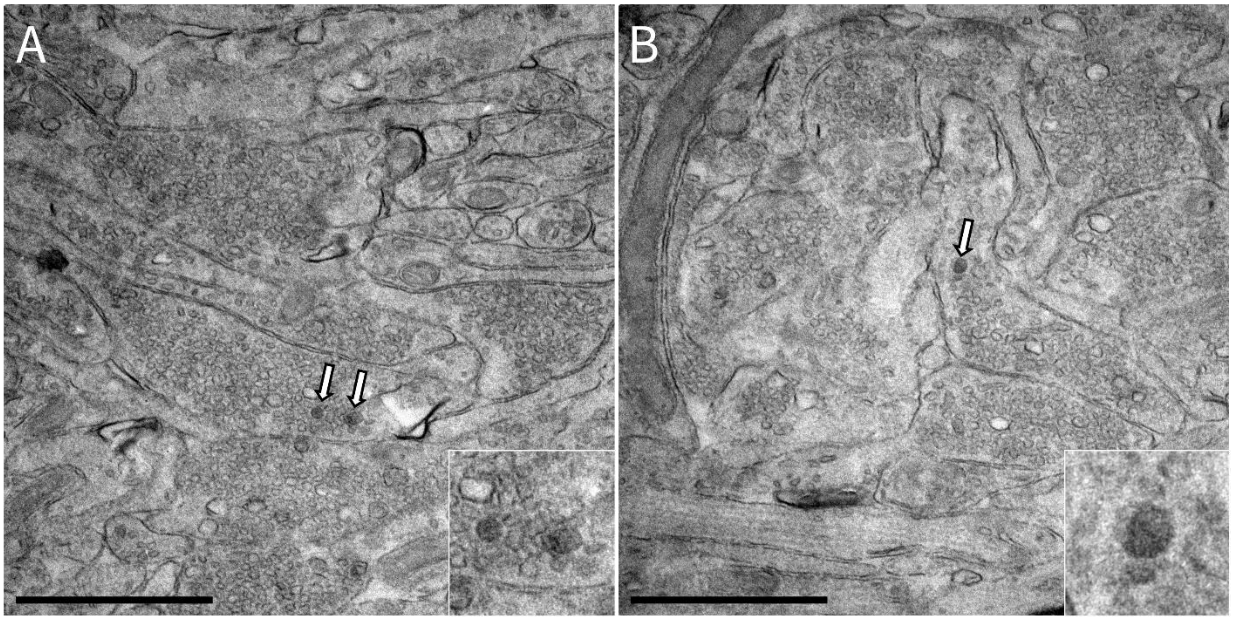

Figure B1. Additional examples of large vesicular profiles with electron-dense cores in non-HRP-reacted AOB glomerular neuropil of *Lithobates catesbeiana*. (A) Transmission electron micrograph showing a presynaptic terminal containing two large vesicular profiles with electron-dense cores (arrows), morphologically consistent with dense-core vesicles, among smaller clear-core vesicles. Inset shows the indicated profiles at higher magnification. Scale bar = 1 µm. **(B)** Transmission electron micrograph showing a presynaptic terminal containing a large vesicular profile with an electron-dense core (arrow), morphologically consistent with a dense-core vesicle. Inset shows the indicated profile at higher magnification. Scale bar = 1 µm. Terminal identity is unconfirmed in both panels as images were acquired from non-HRP-reacted tissue.